EFFICIENT CHARACTERIZATION OF TRANSIENT PULSE SHAPES FROM RADIATION INDUCED UPSETS.

By

William Geoffrey Bennett

Thesis

Submitted to the Faculty of the

Graduate School of Vanderbilt University

in partial fulfillment of the requirements

for the degree of

Masters of Science

in

Electrical Engineering

May, 2012

Nashville, TN

Approved:

Professor Ronald D. Schrimpf

Professor Robert A. Reed

ACKNOWLEDGMENTS

Occasionally a person pursues a path that garners support from everyone around them. I made such a choice, and certain people gave of themselves substantially. Dr. Schrimpf gave my abstract idea a chance, and helped turn it into a reality. This direction was absolutely crucial to the completion of this work. Dr. Reed found ways to keep me funded, the importance of which cannot be understated. The RER group as a whole has brought me through the trenches of learning how to process the physics of radiation effects on semiconductor devices. The RER group at Vanderbilt provides a unique environment that offers resources that are paralleled nowhere else.

Not to be forgotten are those who helped in a non-technical capacity, because sometimes those challenges outweigh any trouble research can create. My friends gave me a time and place to manage my stress and forget about work. My parents created an environment in which college was an expectation, not a choice. When my life tried to divert me, they stepped in to get me back on track. To them I will forever be indebted. Last, but likely most important, is my wife Crystal, who worked while going to school full time to keep our lives comfortable. Hopefully one day I will be able to repay her.

TABLE OF CONTENTS

LIST OF TABLES

LIST OF FIGURES

CHAPTER I

Introduction

Single Events Upsets (SEU) have long been a concern of the space and aviation fields. An SEU occurs when the logic state of a data-storage element in an integrated circuit changes because of the charge generated by a single ionizing particle. In the past, the minimum amount of deposited charge required to cause an upset, Q_{crit}, was relatively large compared to that of present technologies. This kept the focus of the industry on heavy ions that generate relatively large amounts of charge. As devices continue to scale down, the value for critical charge also decreases[3]. This requires consideration of particles that could previously be ignored. Even terrestrial circuits will be exposed to particles that have the ability to upset cells[4]. Finding ways to model these processes is critical for estimating and improving the reliability of circuits.

Critical factors for many currently produced transistor technologies are the magnitude and duration of the prompt current transient generated by a single event strike. The mechanisms of current pulse generation are covered in detail in section I.3. Bistable circuits are often described as having a value for Q_{crit}, which is the amount of charge required to change the state of a node. While this can be true, many of these circuits actually have a critical peak current and a critical charge collected in a short period of time that depend on the properties of the circuit. Characterizing these quantities is the focus of this research.

One of the most accepted ways to model these events is in a finite element solver, such as Technology Computer Aided Design (TCAD)[5]. The solutions given by these simulations are very accurate and rely on the underlying set of differential equations to produce a temporal representation of charge collection. Unfortunately, these highly accurate simulations also require a large amount of processing power. Even utilizing a super computer cluster, a single solution can require days of simulation time. For any design flow that

utilizes iteration, this becomes expensive to implement.

A common solution to this problem is the creation of compact models that closely resemble the full solution, but at a fraction of the time and computation budget. As with any model, assumptions are used to limit the sample space of the solution. This requires the creation of compact models for specific environments, and sometimes the utilization of multiple models to complete a design. Although this adds layers of complexity, it is still significantly more efficient than the full finite element solution. One of the requirements of most compact models is calibration. Creating an appropriate pulse shape that matches the technology of interest is crucial to obtaining an accurate circuit level result.

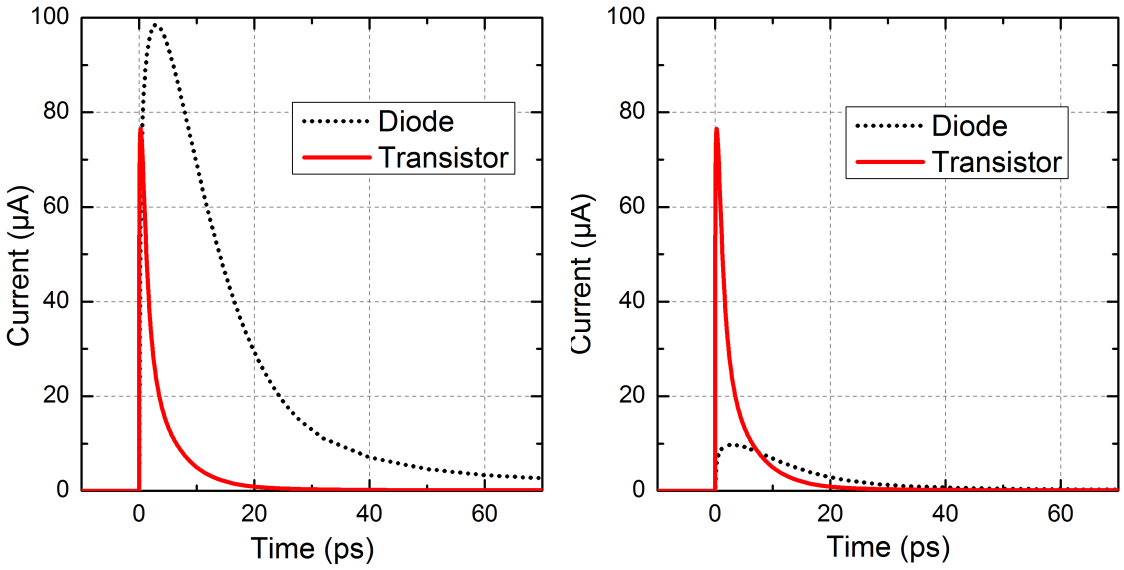

(a) Identical LET strikes.

(b) Identical total charge strikes.

Figure I.1: Comparison of fast transient pulse response of a 45-nm transistor and diode.

The prompt, drift-dominated, section of a single-event current pulse can vary substantially from one technology generation to another. Even different devices in the same technology can have extremely different responses. For example, Fig. I.1a shows two simulated strikes of identical Linear Energy Transfer (LET), in similar technology nodes, but in two different device structures. One is a standard nMOSFET, while the other is a large area

diode. These pulses show how different the responses can be to similar conditions. Assuming one of these shapes, if wrong, could significantly skew the response of a circuit. An example of incorrect calibration is shown in Fig. I.1b. The two pulses were calibrated using simulation data from the TCAD generated pulses shown in Fig. I.1a. To calculate the magnitude of the pulses, the Full Width Half Maximum (FWHM) of the current pulse was normalized to the same amount of deposited charge. The charge in the FWHM of the two pulses is therefore identical, but as can be seen, the resulting pulses have a magnitude difference of around 6x. This significant difference is more than enough to completely alter their circuit level response.

This demonstrates why calibration is necessary for obtaining an accurate circuit-level result. This thesis describes a calibration method for circuit-level current injection based on the physics of carrier transport in p-n junctions. It focuses on relatively low energy deposition (LET < 10 MeV-cm^2/mg) events, allowing for a simplification of the underlying physics. The methodology uses finite-element device simulations for initial calibration, but does not require additional device simulations during the circuit simulation process, allowing pulses to be generated in real time for strikes at different values of LET. This process can be accomplished in substantially less time than a full TCAD approach. A comparison of a result obtained from the presented method to that obtained from a TCAD simulation is shown in Fig. I.2. The "Estimated" pulse is the result obtained from the method presented here. These pulse shapes can be implemented in a compact model for use in circuit-level simulations. This method is not a new compact model, but rather a method to calculate the appropriate fast transient response for a given device structure. This method is highly accurate for obtaining the attributes of the prompt current pulse for implementation into higher level models.

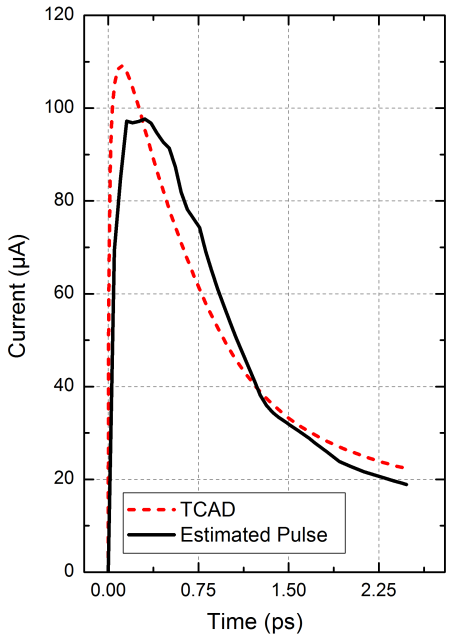

Figure I.2: Comparison of the calculation method presented here and simulation data from TCAD.

CHAPTER II

Background

II.1 Ionizing Energy Deposition

The initial process contributing to a Single Event Upset is ionization. There are two main categories of ionization, indirect ionization, a process by which the incident particle creates secondary particles that then generate electron hole pairs in the struck material, and direct ionization which describes electron hole pair generation resulting from energy loss by the incident particle. Both types of ionization are described here, but this work emphasizes energy deposited by direct ionization.

The three forms of indirect ionization are: Rutherford scattering, elastic nuclear reactions, and inelastic nuclear reactions. Rutherford scattering, sometimes called Coulomb scattering, occurs when an incident particle passes within a small distance of an atomic nucleus. This close proximity allows the like-charge of the two particles to repel each other and deposit energy into the system. The Coulomb forces are what cause the repulsion, and is the source of the name Coulomb Scattering. A nuclear reaction, in general, is an interaction that directly involves the nucleus of an atom. In an inelastic nuclear reaction, the resultant products are physically different from the particles that initiated the reaction. For instance, when an iron ion strikes a silicon nucleus, the result could be a variety of ions other than silicon and iron. An elastic nuclear reaction is related to Rutherford scattering, but the incident particle comes into direct contact with the nucleus. The products from this reaction are identical to those that existed before the reaction occurred.

Direct ionization, while not completely separate from indirect, has a significantly different energy deposition signature. This process deposits almost all of its energy along a vector of the trajectory of the incident particles. During direct ionization, the incident particle generates electron hole pairs by transferring enough energy to a bound electron

to free it. This process is illustrated in Figure II.1. This mechanism has a fairly constant LET over short distances ($< 2\ \mu$m)[6], and can even be accurately estimated over greater distances. This work emphasizes particles that generate relatively low LET tracks (LET $<$ 10 MeV-cm^2/mg).

Alpha particles usually have a sufficient range to penetrate present day depletion regions, and have LET up to 2 MeV-cm^2/mg [7]. There is an abundance of other particles that can create LET values in this range, but the charge-collection process is relatively independent of the particle type. Different particle species have different values for LET, so this work chooses a value for LET that could relate to multiple particle species. In this way, the specific incident particle is not important, just the amount of deposited energy that generates electron-hole pairs.

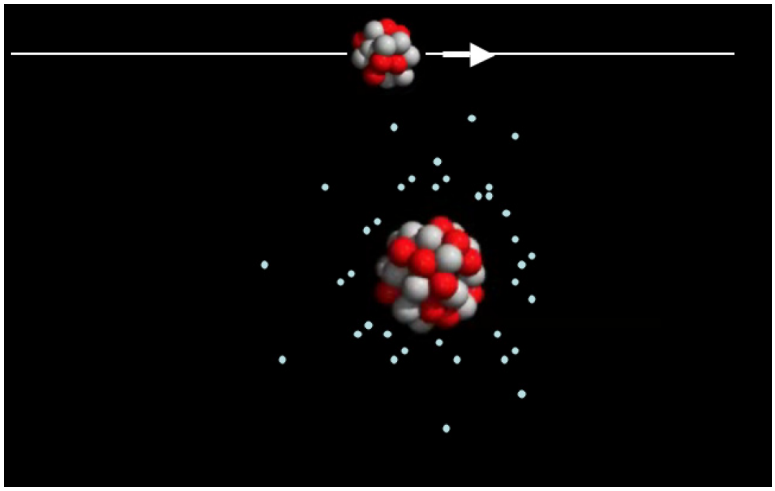

Figure II.1: Process of direct ionization of an incident particle with the electron cloud of a target material[1].

II.2 Carrier Collection Mechanisms

Output current generated from a strike is the single most import factor in determining whether a cell has upset. Determining both the magnitude and duration of a current pulse depends on the fundamental mechanisms of charge transport. There are two mechanisms that contribute to charge transport: drift and diffusion.

Diffusion is a relatively slow process compared to drift. There are two types of diffusion that have a relevant impact on SEU, and those are standard and ambipolar diffusion. Standard diffusion is regularly used in the solution to carrier transport of operating semiconductor devices. This mechanism works from the concept that an excess of carriers in one area results in a net transport of those carriers into regions with a lower density. The equation for this transport method can be seen in II.1, where μ is the carrier mobility, D is the diffusion coefficient, and $\frac{dn}{dx}$ is the change in carrier concentration versus distance.

$$J_{Diff} = \mu D_n \frac{dn}{dx}, [8] \tag{II.1}$$

Ambipolar diffusion is a special case of standard diffusion by which oppositely charged carriers in a plasma diffuse at the same rate because of the electrostatic attraction between the particles. In silicon, this causes electrons to diffuse slower, while increasing the diffusion of holes. This is a special case of diffusion that is only relevant here due to the ability of high energy particles to create plasma columns when they strike a device. Due to the energy restrictions placed on this work, ambipolar diffusion is not a dominant mechanism in the collection process.

Drift is typically a faster process than diffusion. Drift is enabled by an electric field being present in a material. Carrier transport caused by drift acts on electrons and holes in an opposing manner. Electrons move towards regions of higher potential, while holes are attracted to regions that have lower potential. This causes electron hole pairs deposited inside an electric field to be separated in opposite directions. The equation for drift current can be seen in II.2. A concept related to drift current is that of carrier drift velocity, the speed at which a carrier moves due to the presence of an electric field. In silicon, the drift velocity saturates at approximately $1 \cdot 10^7$ cm/s. Equation II.3 shows drift velocity, accounting for saturation. For completeness, the total current equation is given in Eq. II.4 as the sum of drift and diffusion. For the incident particle energies considered in this work,

diffusion is rarely a significant collection mechanism, but it is included in the calculations to encompass as many cases as possible. Eq. II.5 gives the final equation needed to see how drift and diffusion play a role in the calculation of the carrier velocity, or transport.

$$J_{Drift} = qn\mu E, [8] \tag{II.2}$$

$$v_D(E) = \frac{\mu E}{1 + \frac{\mu E}{v_{Dsat}}}, [8] \tag{II.3}$$

$$J_{total} = qn\mu E + \mu D_n \frac{dn}{dx}, [8] \tag{II.4}$$

$$v_{electron} = \frac{J_{total}}{qn} = \mu E + \frac{\mu D_n}{qn} \cdot \frac{dn}{dx}, [9] \tag{II.5}$$

Drift and diffusion are fundamental to all semiconductor devices, but in radiation environments there are several mechanisms that can play a unique role. Conduction through a plasma can occur when the incident particle generates enough carriers along a path extending away from the drain of a transistor to allow that path to become highly conductive. Carriers travel along the column at a higher rate than they do radially away from the column center. When this column extends through a region of high electric field, like a reverse biased junction depletion region, an enhancement of charge collection can occur [10].

Likewise, tracks with high carrier densities can create regions outside of the track that inhibit carrier motion. This is most prominent when the ion track travels through the depletion region and extends well into the substrate. A barrier is established, caused by carrier gradients and thus an electric field, below the track (in the substrate) that inhibits majority carriers from entering into the substrate, and can allow for a higher percentage of charge to be collected at the junction, due to a lack of recombination[11]. While both of these effects can strongly affect circuit operation, they require a relatively large amount of energy to be deposited, and these energies are well outside the scope of this work. These collection mechanisms are omitted from the model presented.

II.3 Basic Single Event Carrier Collection Example

A simple overview of current generation from a single event strike aids in the understanding of this work. A p-n junction diode with an incident ion is shown in Figure II.2a. The strike is normal to the junction, and all electron hole pairs are generated by direct ionization. For lightly ionizing strikes, the field in the depletion region remains stable and immediately begins transporting electrons to the n-type material and holes to the p-type material. As discussed before, this process is fast, and leads to the generation of a current pulse that is often known as the prompt current pulse. The prompt component of a generated current pulse is labeled in II.2b. Following the prompt collection, a transition to diffusion-dominated collection occurs. There is not a hard geometrical boundary for this location, rather a range over which drift becomes less dominant. The region, sometimes called the diffusion tail, is labeled in II.2b. The distance a carrier can diffuse before recombining is referred to as the diffusion length. On average, in the energy range considered here, carriers that are within one diffusion length of the depletion region can be collected by diffusion.

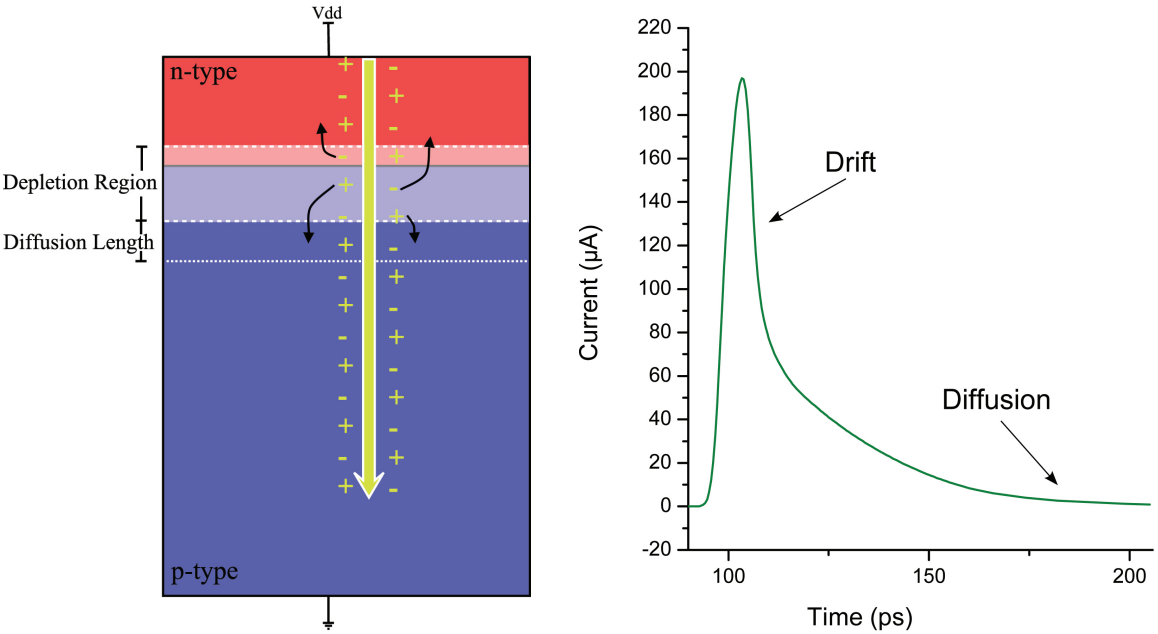

(a) Collection from an ion strike is illustrated for a basic p-n junction.

(b) The resultant current pulse is shown for the strike in part (a).

Figure II.2: Ion strike and resultant current pulse

II.4 Previous Compact Model Work

Compact modeling is the process by which complex systems are described by a set of simplified equations. In circuit design, a model describes the operation of a semiconductor device as a function of input conditions. These models are used due to the complexity and computational expense of obtaining a finite element solution for every event. Compact models at their most basic level are implemented in every SPICE level circuit simulation software. Each device, transistor, etc., is described by a basic set of equations that are approximations of the full device solution. This enables circuit designers to work on the scale required to design useful circuits.

Radiation hardening of circuits has often lent itself to compact models to test the effects of radiation on circuit design. To obtain a statistically valid set of events, thousands or even millions of events may be required. Although conceptually different than a SPICE compact model, an example of a compact model used for radiation hardening is the nested

sensitive volume model designed by Warren et al.[12]. In the nested volume model, a set of concentric, nested sensitive volumes are used in MRED (Monte Carlo Radiative Energy Deposition)[13]. MRED is a simulation tool that calculates the amount of energy that has been deposited in a volume due to the interaction of an energetic particle. Each volume is given an efficiency, the percentage of total deposited charge that is collected as current on the node of interest, and a time at which it contributes to a current pulse. Calibrating these volumes correctly allows current pulse shapes to be generated in a circuit for a given incident particle. This process can be run in series with a circuit simulation tool to produce a statistical representation of the circuit's robustness. Some similar concepts are implemented in this work.

Kauppila et al.[2] designed a compact model that could be utilized to implement the efficient calibration method presented in this thesis. This model is a modified current source that responds dynamically to circuit conditions. The current source checks the bias condition on the connected node, and adjusts the amount of injected current accordingly. A comparison of TCAD mixed mode simulations and an assumed double exponential SPICE simulation is shown in II.3. The independent double exponential was calibrated using an ideal TCAD simulation, and was implemented in SPICE without accounting for the changes in bias conditions at the node of interest. The output from this model produces more accurate results, closely matching the black Mixed Mode TCAD curve shown in II.3, but maintaining a compact model form. This compact model's importance is its ability to take an ideal response of a node and match the response of the circuit with appropriate bias conditions. This is also why it can be used in conjunction with the efficient calibration method presented here.

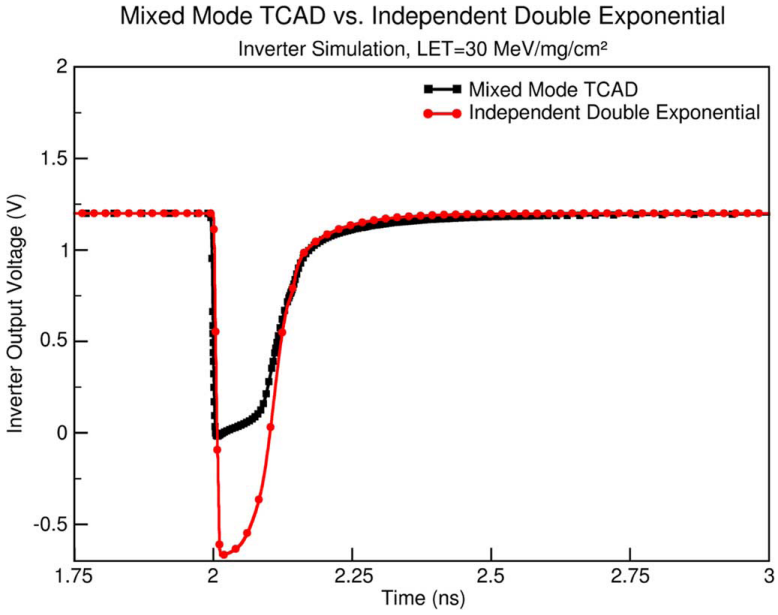

Figure II.3: Output comparison TCAD mixed mode simulations and an assumed double exponential SPICE simulation[2].

CHAPTER III

Device Simulation Environment and Calibration

III.1 Device Models

Keeping track of the motion of individual particles in a semiconductor device is extremely complicated. The solution is to calculate the net movement of a group of carriers to determine device operation. These differential equations are the basis for TCAD. TCAD typically uses a finite element solver, meaning that it creates a grid of points in space for which it finds a solution. This grid of space is referred to as the device mesh. For every step in time, TCAD obtains a solution for every point in the grid. The required time steps can easily be less than a femtosecond and the number of points in a 3-dimensional mesh can be well above $1 \cdot 10^6$. For complex devices, transient 3D solutions can be daunting, and can even become impossible. A solution from a TCAD simulation is the standard for comparison of this work. The sections that follow describe the calibration of the TCAD models used for comparison.

Heavy-ion simulations were run in TCAD. The heavy-ion command uses a value of constant LET to generate carriers along a track vector. The track vector location and direction allow for full control in directly comparing with energy deposition results in MRED. In 3D, TCAD generates a radial Gaussian distribution profile of carriers along the track vector. The generation function is also Gaussian in time; these Gaussian profiles allow for smooth transitions and efficient solution. An example of the heavy-ion command is shown in Figure III.1. The track radius is 50 nm, the LET is 2 MeV-cm^2/mg, and the characteristic value, S_{hi}, of the Gaussian generation function, Eq. III.1, has been set to $2 \cdot 10^{-13}$ s.

$$T(t) = \frac{2 \cdot exp(-(\frac{t-t_0}{\sqrt{2} \cdot S_{hi}})^2)}{\sqrt{2} \cdot S_{hi} \sqrt{\pi} \cdot [1 + erf(\frac{t_0}{\sqrt{2} \cdot S_{hi}})]}, [5]. \tag{III.1}$$

This generation time helps resolve the physical collection mechanisms with greater clarity

than the default value, $2 \cdot 10^{-12}$ s. As discussed in section III.2.2, there is no physical basis for this generation window, because the mechanisms behind carrier generation are orders of magnitude faster than the default generation window. The default has only recently become an issue due to the increasingly fast single-event response of modern technologies. If the device response time is similar to or faster than the time over which charge is generated in simulation, then significant distortion of the collected current pulse can occur. Examples of temporal distortion of carrier generation are given in section III.2.2.

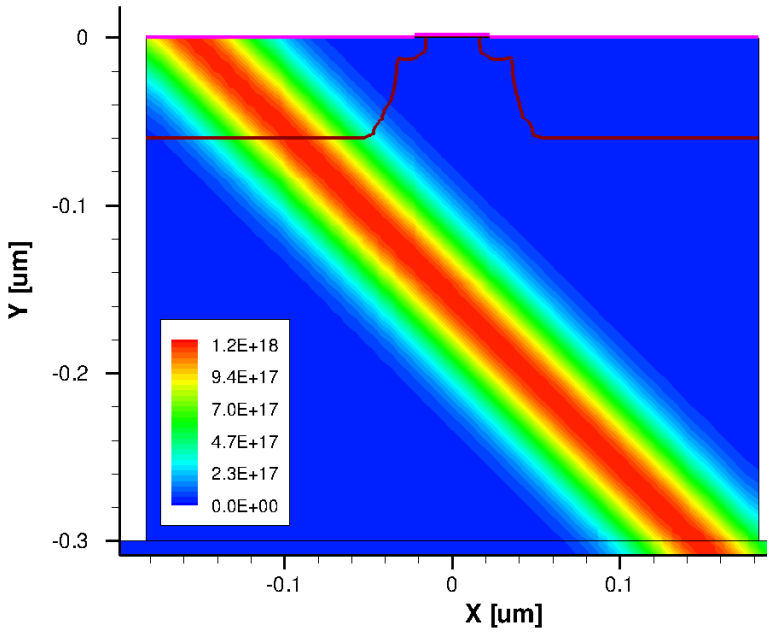

Figure III.1: Example charge generation track from the heavy-ion command in TCAD. Strike is at an LET of 2 MeV-cm^2/mg and is at an incidence of 45 degrees.

III.1.1 45nm nMOSFET Transistor

The central device considered in this work is a 45 nm nMOSFET transistor that is modeled after design notes for an Intel-based fabrication process[14]. This design note details a process simulation that attempts to match both the structure and operation of Intel's process. The output of these simulations created the basis for the device structure. This device was chosen due to its present relevancy, but the scope of the calibration method presented is

not limited to this device. Electrical characterization was performed using current and voltage sweeps provided from manufacturer specifications. The goal for this process was not to obtain a flawless match of the actual device, but rather a close representation that responded realistically.

The device structure is shown in Figure III.2a. The source and drain are highly doped ($5 \cdot 10^{19}$ cm^{-3}), and have a depth of approximately 60 nm. Shallow Trench Isolation is present on the outside of the source and drain, but is not shown. The channel and threshold voltage implants peak at $6 \cdot 10^{18}$ cm^{-3}. The substrate has a constant doping of $1 \cdot 10^{17}$ cm^{-3}, excluding the substrate contact region which has a Gaussian peak of $1 \cdot 10^{18}$ cm^{-3}. Both source and drain have identical Lightly Doped Drain (LDD) regions that peak at $9 \cdot 10^{18}$ cm^{-3} but only extend 15 nm away from the surface. The gate is constructed from a 1.5 nm thick SiO_2 insulator with a high-k metal gate. The gate metal has an effective work function of 3.44 eV [15].

Some physical attributes of a manufactured device are not visualized for simplification, because they do not contribute to the single event response. Such features include surface oxides that are made as part of the doping process. Contacts have also been idealized.

III.1.2 Large Area Diode

A second device was also used to verify the calibration method presented here. This is a large area diode that is shown in Figure III.4. The n^+ cathode is doped at $1 \cdot 10^{20}$ cm^{-3} and extends 120 nm from the surface contact. This region is on top of a p-type substrate with a doping of $5 \cdot 10^{17}$ cm^{-3}. Doping profiles and the device geometry can been seen in Fig. III.4.

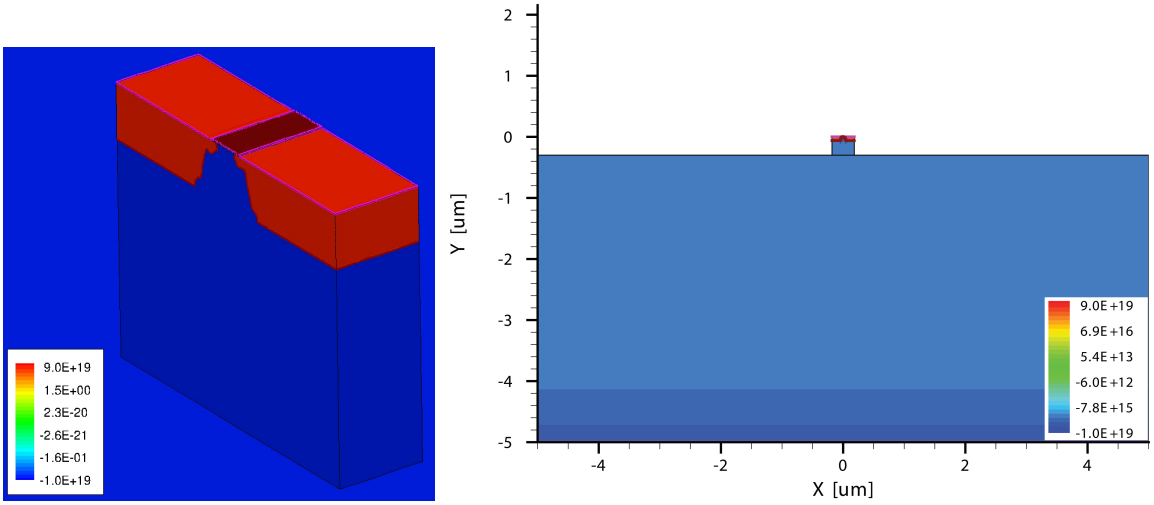

(a) 3D view of the transistor position and geometry.

(b) 2D view of the full device including substrate.

Figure III.2: 45-nm transistor used in this work.

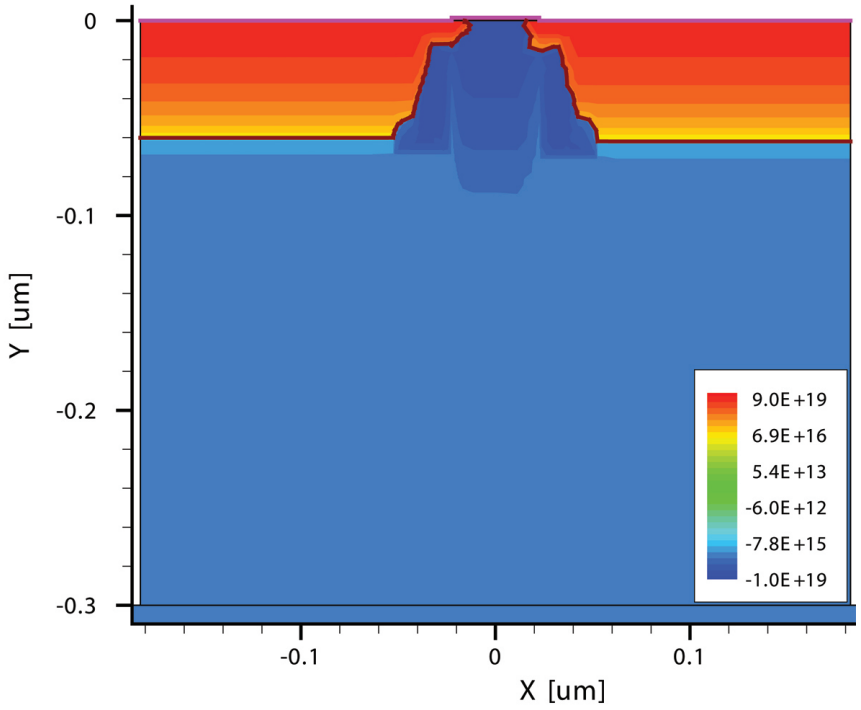

Figure III.3: Close-up image of the doping profile for the 45-nm nMOSFET.

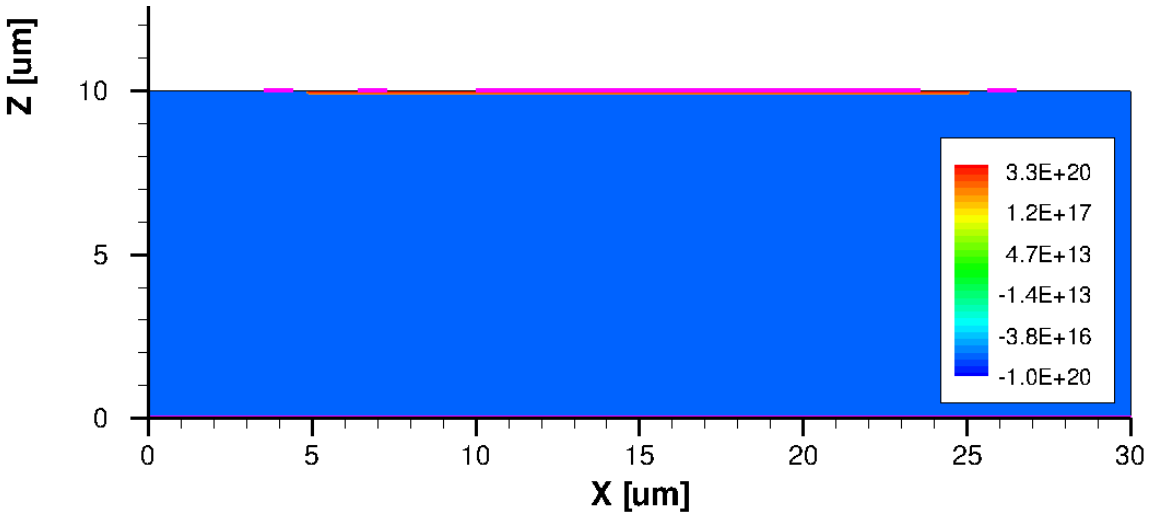

(a) 2D view of the full diode

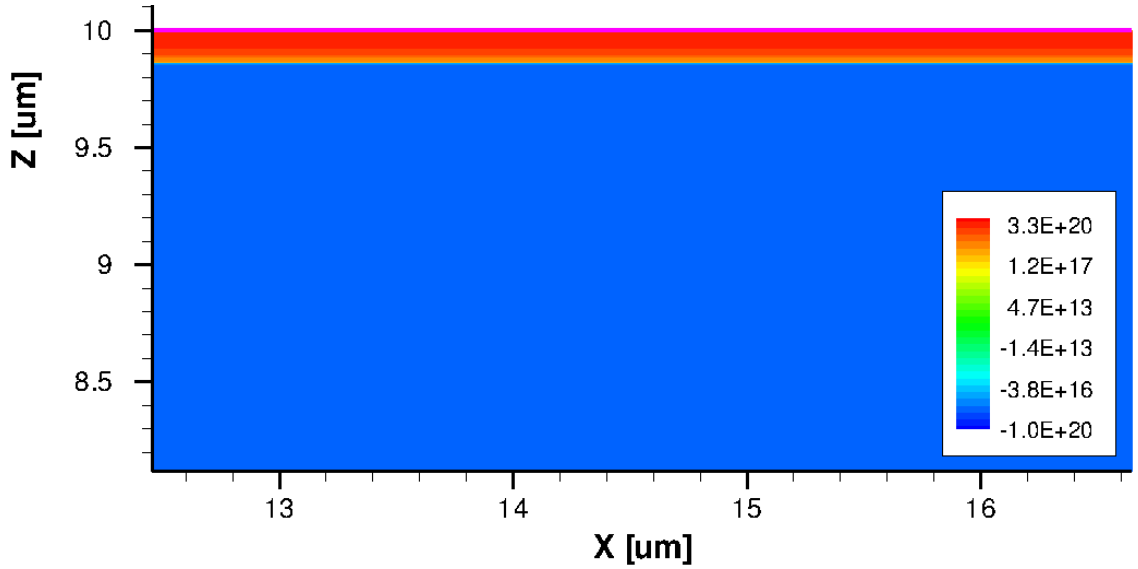

(b) 2D close-up view of the n^+ doping profile in the large area diode.

Figure III.4: Large area diode doping profiles

III.2 Energy Deposition

III.2.1 Quantity of Charge Deposited

In contrast to TCAD, MRED takes a single incident particle passing through material and calculates the amount of energy deposited inside of the material. MRED does not describe the transport of thermalized carriers, but rather works at the material level to describe the interaction between a target material and incident particle species. For this work, a simple silicon slab was used for the charge deposition calculations. A volume that describes the space from which charge is collected during the prompt current pulse was created in MRED, discussed later in detail, and was implemented to determine the magnitude of the output current pulse.

To guarantee strikes inside the region of interest, particle vectors were forced to pass through a specific point in space. This allows for a wide range of track vectors, but with a very high yield from strikes of interest. This also allows for direct correlation to the heavy-ion command in TCAD. By knowing where the point is located, and the angle of incidence, an identical vector can be created for the particle in TCAD.

III.2.2 Temporal Characteristics

It is often approximated that particle-induced charge generation occurs instantaneously. While this may be appropriate, depending on the frame of reference of the mechanism being researched, it is not always accurate in the reference of a fast transient pulse[16]. The default characteristic value of the Gaussian deposition time in the heavy-ion command used by TCAD is $2 \cdot 10^{-12}$ s. There is no physical evidence cited by Synopsys for this value, but was most likely chosen because it was much less than the radiation response of devices at the time of its creation. For fast transient pulses that occur during time periods several times larger than this, it is an appropriate choice for deposition. If however, the duration of the prompt response of the p-n junction is close to or less than this value, distortion may occur. This distortion is analogous to errors caused by the sampling of a continuous

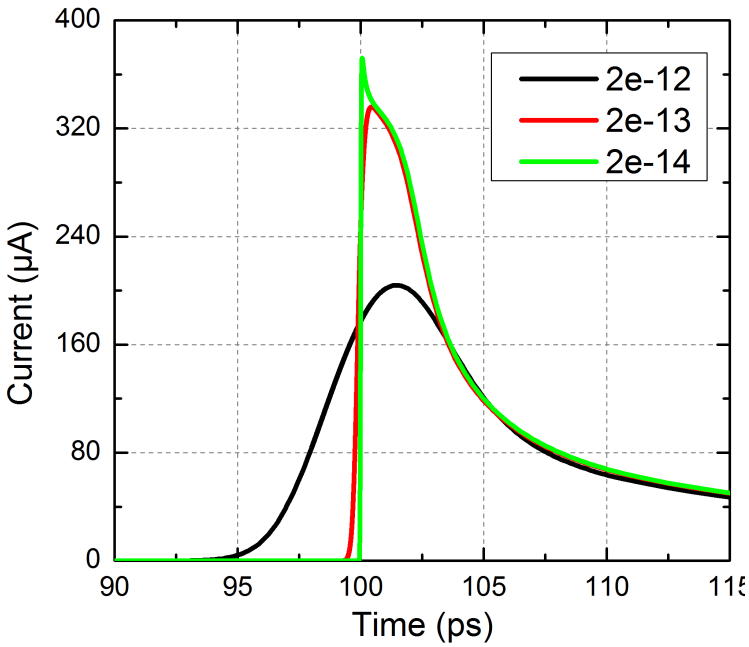

Figure III.5: Resultant current pulse for three different generation times.

waveform. If the waveform is smaller than the sample period, the recorded signal will be inaccurate. An example is shown in III.5, which represents the particle-generated current vs. time for three different generation time constants.

The drain of the transistor used to obtain the waveforms in Fig. III.5 is biased at 1 V while the source and substrate are grounded. The characteristic value of the generation Gaussian was varied from $2 \cdot 10^{-12}$ to $2 \cdot 10^{-14}$ s to see the response of the circuit. $2 \cdot 10^{-14}$ s is not a physically realizable value. Almost every type of incident particle would take longer than this value to traverse the region of interest in the device, making it impossible for the particle to deposit its energy in this time period. It is shown here as an example of the ability to shrink the generation time too much and create distortion in the other direction. The ability to generate unphysical results from TCAD simulations has been detailed in [17]. A plot of the generation rate as a function of time is shown in III.6.

One such issue can be seen in Figure III.5 as a spike when using the shortest generation time. This is caused by an unrealistic generation time, coupled with an ideal contact, and

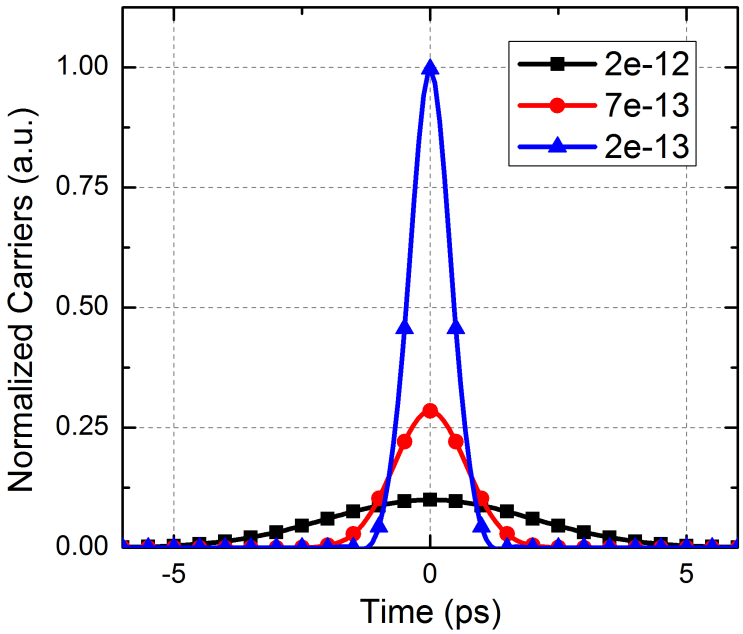

Figure III.6: Generation rate as a function of time is shown for three generation times.

the boundary requirement of the simulator tool to hold the electron concentration equal to the background doping at the boundary. A diffusion current is generated because the simulator must hold the carrier density at the boundary constant, regardless of the injection level. The actual mechanisms behind this do not need to be fully understood, only that there can be distortion caused by generation times that are unphysical. This current is extremely short lived, and is an artifact of the generation time chosen, and the use of a finite element solver.

The velocity of the incident particle should be considered to obtain accurate results. Many junctions are so small that the velocity is not extremely important, but in some device structures, the particle's velocity could have a significant effect. The velocity of the particle is obtained from the kinetic energy equation,

$$E_k = \frac{1}{2}mv^2, [9]. \tag{III.2}$$

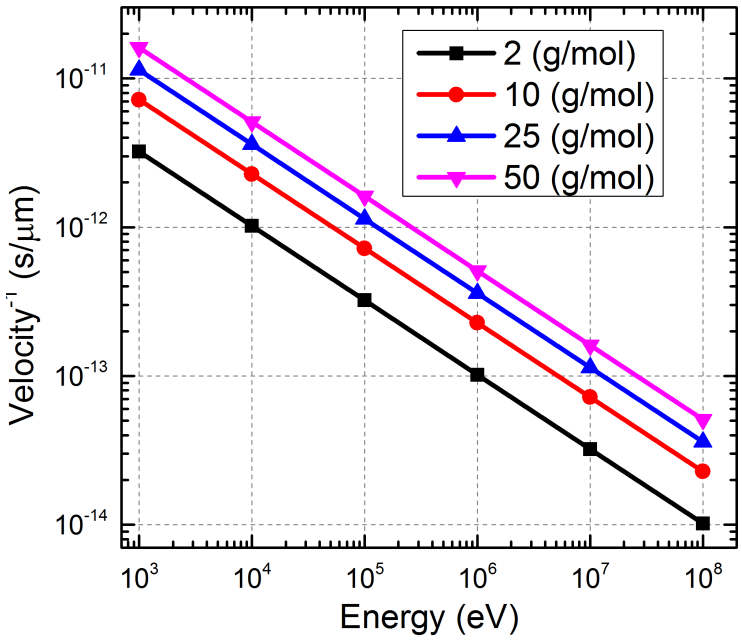

Figure III.7: Time to travel one μm as a function of particle energy is shown for four different atomic masses.

Fig. III.7 gives the time it takes an incident particle to traverse 1 μm. This is given as an absolute minimum generation time because it is easily calculated. To calculate the actual deposition time, every secondary electron would have to be tracked, until it thermalized with the silicon band structure. This would require a Monte Carlo simulator like MRED that kept track of time; this software is not readily available. So, choosing a value significantly slower than the particle's velocity serves as a good lower limit. Plots for several masses and energies are given as a reference for choosing an appropriate generation time. Some of the slower moving particles could still have a significant LET, while taking longer than the generation time to traverse the junction responsible for generating the fast transient pulse. This is not a major concern for the default generation time in TCAD, $2 \cdot 10^{-12}$ s, but could become a significant source of distortion if a value of generation time is chosen to be too small relative to the actual particle velocity. The goal when selecting a deposition time is to find a value that is several times larger than the traversal time of the incident particle, but also several times smaller than the device response. For this work, a value of $2 \cdot 10^{-13}$ s

was chosen, and is used in the subsequent results. Results are not extremely sensitive to this value; even four or five times higher or lower will give approximately the same result. The main goal is to avoid picking values at the extremes for modern technologies. $2 \cdot 10^{-13}$ is a conservative value because most particles will traverse modern depletion regions in femtoseconds, and most of the secondary electrons will thermalize in tens of femtoseconds, allowing for an order of magnitude buffer in the generation time period.

CHAPTER IV

Efficient Calibration Method

IV.1 Method Overview

The goal of this work is to obtain a relatively accurate description of the fast transient pulse with a minimum amount of simulation or engineering time. As discussed previously, focusing on low LET particles and the prompt response of the device, allows for simplification of the charge collection mechanisms resulting from a single event strike. The following section describes the process of calibrating a pulse, and generating a circuit-level signal from a charge deposition profile in MRED. The process flows from device calculations to charge deposition in MRED and ends at current pulse generation in a circuit level simulation.

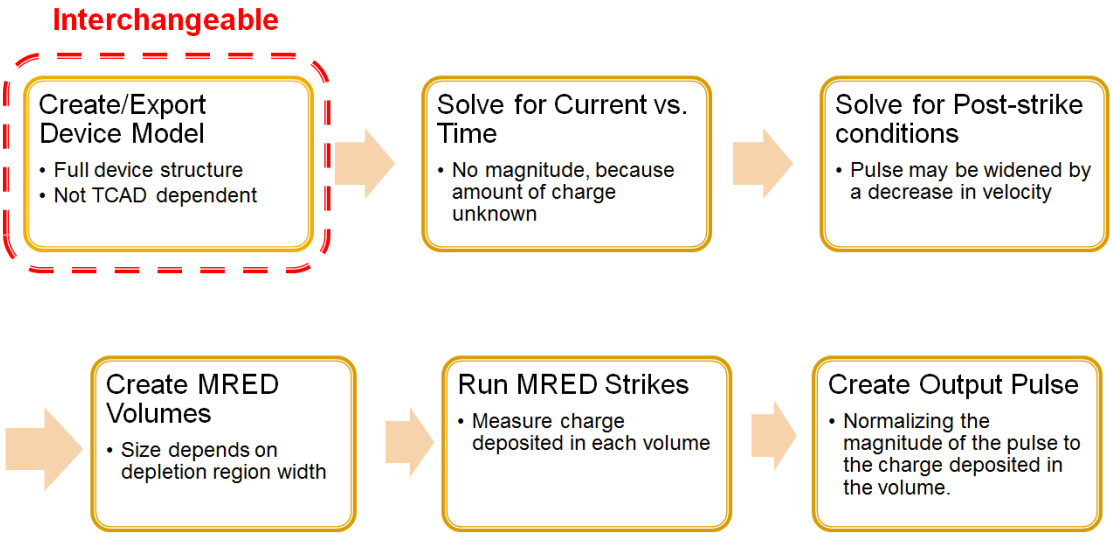

Figure IV.1: Flow chart for the presented characterization method.

IV.1.1 Concept

A discussion of charge transport, and ultimately device current, will aid in the understanding of the derivation of the presented method. Fig. III.2, discussed previously, showed

the basic transport of ion-generated charge. Outside of the silicon device, the simulator assumes ideal transmission of current, meaning that charge transport happens instantaneously from the power source to the silicon device. Charge transport inside of the silicon is not instantaneous, and gives rise to a transport time, as well as the device current, for charge generated from an ion strike.

At the moment of generation, the deposited charge sets into motion an extremely fast current know as a displacement current. This current is a function of changing electric fields induced by the deposited charge, and not by the transport of the deposited charge. An example of a displacement current caused by a point source, as it pertains to single-event strikes, is shown in [18]. This current contributes relatively little total charge when compared to the total collection from the ion strike, and occurs when there is isolated charge away from the biased contact. For the case of a strike that traverses the active region of the transistor, the charge is not sufficiently separated to create a significant displacement current at the contact. This current can therefore be omitted to obtain a simplified solution.

The current that remains to be calculated in the semiconductor results from the transport by drift and diffusion discussed previously. This work concentrates on calculating the net movement of a group of carriers. The separation and transport of carriers by a strong electric field inside the reverse biased depletion region occurs on a very short time scale, and is responsible for the prompt current transient. Current density is defined as the amount of charge that passes through a plane in space per unit time. For the case of the reverse biased diode, the plane of interest is typically the cathode contact on the n+ diffusion. To calculate the current density, and ultimately the total current, the amount of charge that passes through the plane of interest, over a specified time, must be determined.

This can be accomplished by equally segmenting the semiconductor along the direction of current flow, pictured in Fig. IV.2. If a constant electric field is applied across each segment of the device, causing the generated electrons to move due to drift, they will have an average carrier drift velocity, v_d. The time it takes carriers generated at the beginning

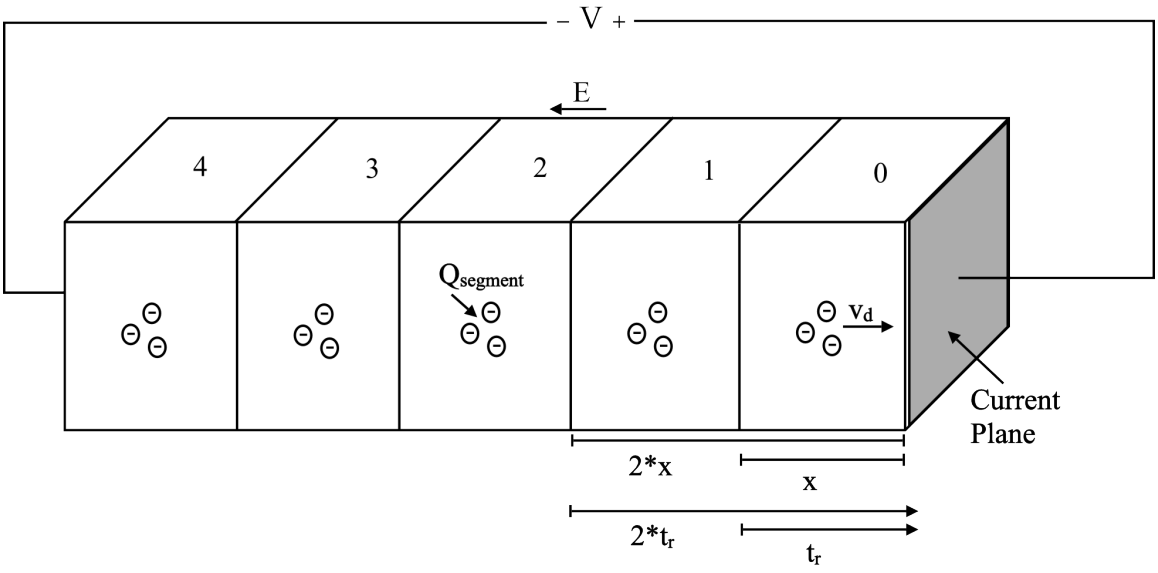

Figure IV.2: Segmented device with a constant deposited charge, and constant drift velocity.

of each segment to reach the current plane can be calculated using the distance they must travel to reach the plane, divided by their velocity in the region they must traverse. This is known as the transit time t_r. Charge generated in segment 1 takes $1*t_r$ to reach the plane, while charge generated in segment 2 takes $2*t_r$, and so on. The time between the arrival of charge in consecutive segments is t_r. If an equal amount of charge is deposited in each segment, $Q_{segment}$, the average current is given by,

$$\frac{Q_{segment}}{t_r}, \tag{IV.1}$$

because $Q_{segment}$ passes through the plane in time t_r. The same concept can be applied to holes moving in the opposite direction.

A simple extension of this example is to vary the amount of charge deposited in each volume, as shown in Fig. IV.3; thus $Q_{segment}(1)$ is the amount of charge in segment 1, while $Q_{segment}(2)$ is the amount of charge in segment 2, and so on. There is still an assumption that diffusion is minimal when compared to drift. Therefore, the average current at time

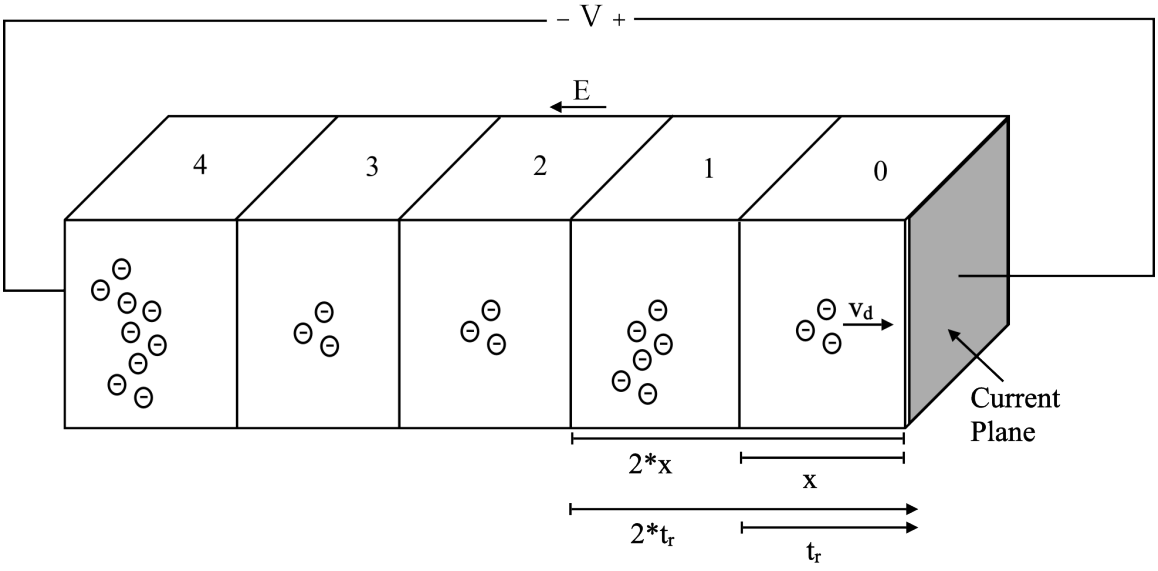

Figure IV.3: Segmented device with a variable deposited charge, and constant drift velocity.

1*t_r is $\frac{Q_{segment}(1)}{t_r}$, and likewise $\frac{Q_{segment}(2)}{t_r}$ at time 2*t_r. This creates a current density that changes with respect to time, either increasing or decreasing with respect to the amount of charge deposited in each segment.

A final extension, which leads to the method presented in this thesis, is to alter the example such that $Q_{segment}$ and the electric field both vary for each segment, shown in Fig. IV.4. This assumes that each segment has a separate value for electric field, which causes the electron velocity, and subsequently the transit time, to vary. In this example, t_r is no longer constant, but assumes values $t_r(1)$, $t_r(2)$, etc., for segments 1, 2, etc. Therefore the current between times $t_r(0)$ and $t_r(0)$+$t_r(1)$ is $\frac{Q_{segment}(1)}{t_r(1)}$, and likewise $\frac{Q_{segment}(2)}{t_r(2)}$ between $t_r(0)$+$t_r(1)$ and $t_r(0)$+$t_r(1)$+$t_r(2)$. The power supply, contacts, and heavily doped diffusion can be approximated by a single conductor, so the current flowing through the reverse biased depletion region into this conductor represents the majority of current of the system. Similar concepts for current pulse calculations were applied to photodiodes in [19] and [20].

A simulation to show the effects of the electric field on the prompt current transient

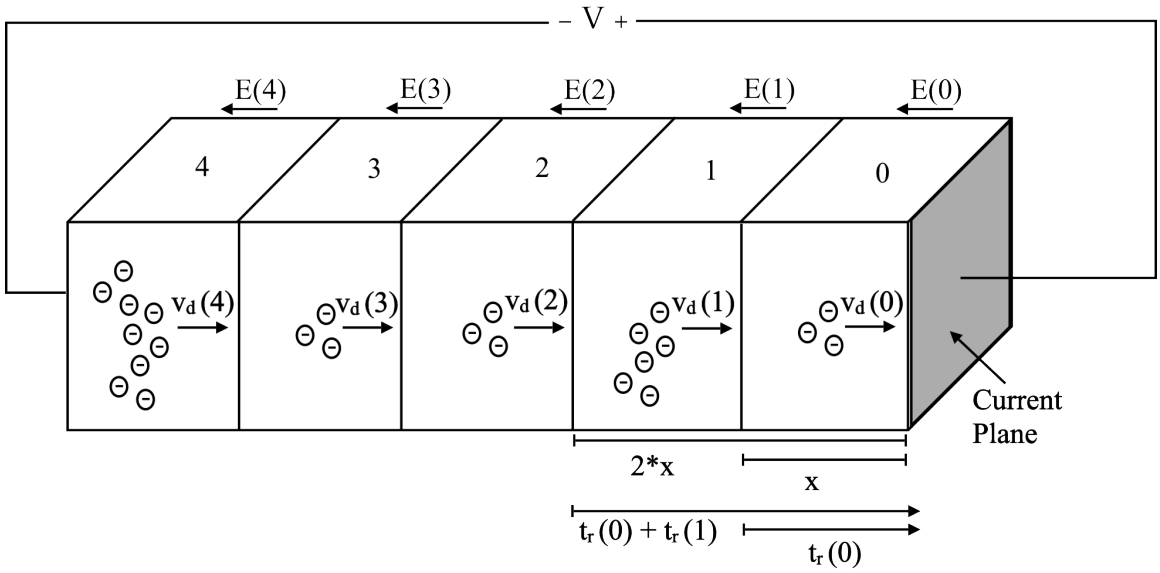

Figure IV.4: Segmented device with a variable deposited charge, and variable drift velocity.

was run by generating ion tracks normal to the drain of a biased nMOSFET. The carrier generation tracks start at the surface of the drain and are terminated at different depths, or distances along the track vector (shown as the yellow arrow in Fig. IV.5a). The current obtained from simulation is plotted vs. time in Fig. IV.5b. The 0.1 μm depth corresponds approximately to the generation track terminating in the middle of the depletion region. The peak current is essentially the same for all strikes that penetrate completely through the depletion region, in this case 0.2 μm and deeper. This shows that the form of the electric field inside the depletion region is the major contributing factor to the shape of the fast transient current pulse. There are other mechanisms, i.e., diffusion, involved in the collection of carriers, but the electric field in the depletion region has the greatest impact on the pulse shape. For the sample space considered in this thesis, charge deposited outside of the high electric field region does not significantly affect the magnitude, duration, or shape of the fast transient pulse.

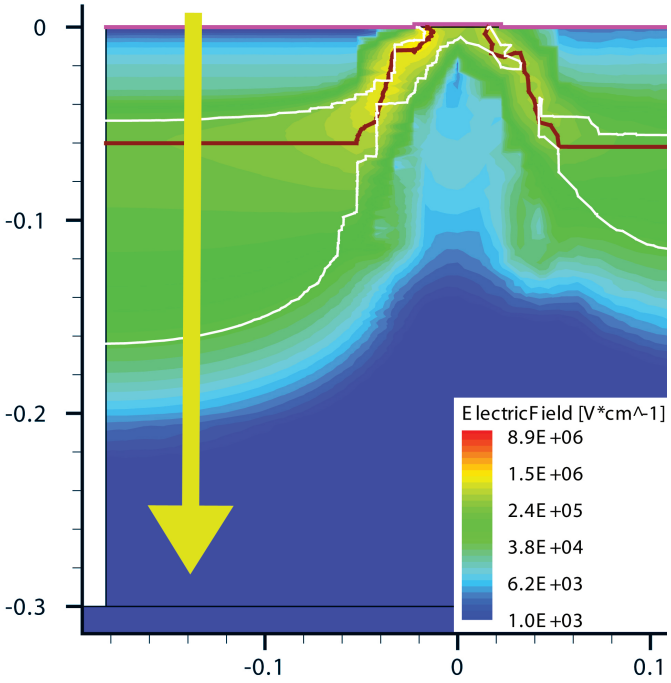

(a) Heavy-ion strike location

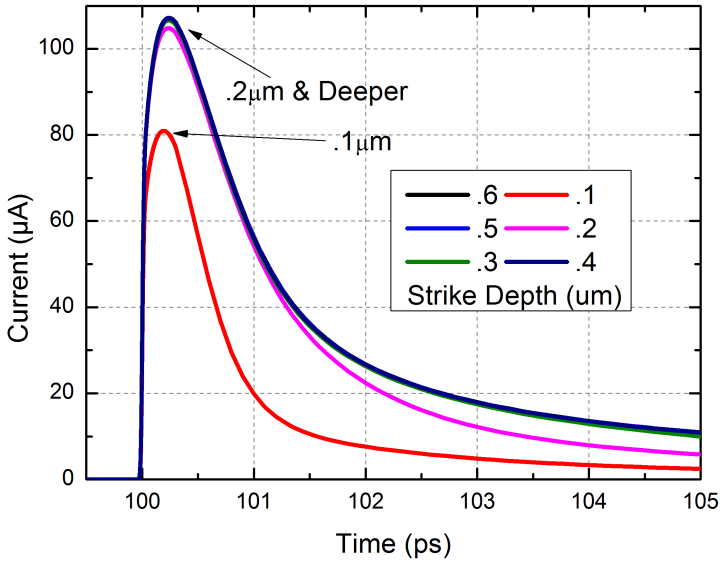

(b) Current pulses resulting from ion tracks of different depths.

Figure IV.5: Current pulse and strike location for various track lengths.

IV.1.2 Data Input

The following terms are used in discussion of this method:

Data Slice 1D series of extracted device data taken at the slice location. This is identical to the 1D chord, and for most device geometries, is a vector normal to the contact. It should contain the following values: doping levels, electric field, and mobility values as a function of distance.

Slice Location Location in the device model where the data for the calculation is extracted. This should begin at the collection contact, and terminate well into the device.

Device Model Geometry, doping profiles, and simulated bias conditions for the device of interest. For this thesis TCAD was used, but is not a requirement.

T(x) A function that returns the time it takes for a carrier at distance x to reach the current plane, location 0, i.e., be collected, in units of s.

v(x) Velocity of carriers at the location x, in units of cm/s.

x(t) Distance from the current plane that takes time t for deposited charge to reach the current plane, in units of cm.

LET$_{si}$ Charge per unit distance, in units of MeV-cm^2/mg.

The minimum amount of information required to utilize this method to characterize the single event response of a reverse biased junction is a 1D slice, or chord, containing the electric field, mobility, and doping levels as a function of distance. This chord is typically normal to the surface for planar devices, and taken at the center of the biased diffusion. For devices with geometries and doping profiles that do not vary significantly in the width direction, a 2D representation of the device is sufficiently accurate. This 2D representation is sliced into a series of 1D chords that become the input into the following calculation process. A slice can be seen in Fig. IV.6, as well as the discrete mesh points of the device

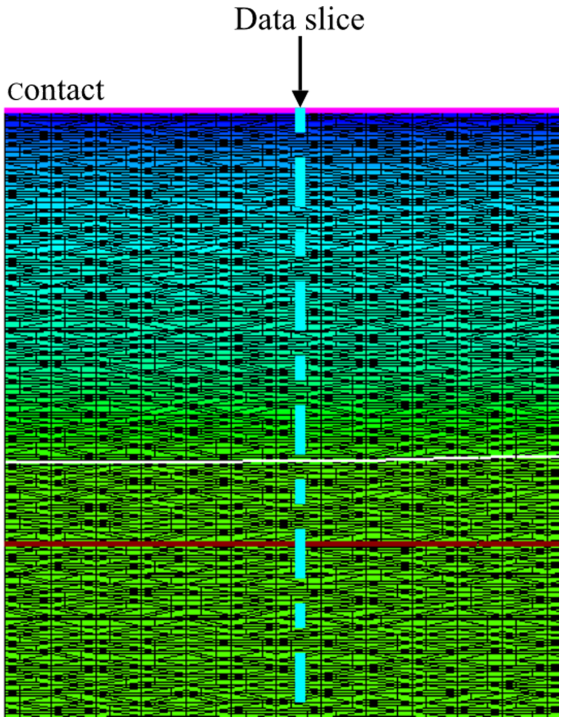

Figure IV.6: Device model used for data extraction is shown with finite element mesh overlaid.

model. In a nMOSFET, the 1D data slice should be taken such that it follows the decreasing potential towards the substrate. For most devices, this vector is normal to the contact, but this could be different depending on the structure being simulated.

Once a carrier passes into the biased diffusion, via the depletion region electric field, it can be considered collected. As discussed in section IV.1.1, once the carrier has reached the current plane, the contribution to the output current is known. To account for this, the location of the depletion region edge in the collection diffusion, $x(d_{n0})$, is set equal to the starting value 0. In this way, any points less than $x(d_{n0})$ are truncated, and not used in the following calculations.

IV.2 Calculations

To determine how minority carriers move as a function of distance, a solution for velocity is needed. The velocity is the speed at which a group of electrons is moving; this can also

be thought of as the average speed of an electron at a given location. The velocity of an electron is given by the equation [9]:

$$v_{electron} = \frac{J_{total}}{qn} = \mu E + \frac{\mu D_n}{qn} \cdot \frac{dn}{dx}. \tag{IV.2}$$

E is the electric field, n is the electron density, D_n is the diffusion co-efficient, q is the charge of an electron, and $\frac{dn}{dx}$ is the change in carriers as a function of distance. As discussed previously, the electron velocity saturates at $1 \cdot 10^7$ cm/s. The electric field is given by the change in potential over distance,

$$E = -\nabla V. \tag{IV.3}$$

The Del operator (∇) in the one dimensional case is equivalent to the standard derivative operation. The last value needed in Equation IV.2 is the carrier mobility. Electrons and holes have different mobilities in the same material, thus the carrier of interest must be known. In an nMOSFET transistor the carrier of interest is the electron, and in a pMOSFET it is the hole. In this thesis the Masetti Doping Dependent, Conwell-Weisskopf Carrier to Carrier Scattering, and High Field Saturation mobility models were used; their implementation is detailed in [5].

Transit time is defined here as the time it takes a carrier at a given distance to be collected. For the example of an nMOSFET, it is the time it takes an electron to travel from its generation location to the current plane along the data vector. The function that calculates this value is given by integrating the reciprocal of the velocity over the distance needed to travel.

$$T(x) = \int_0^x \frac{1}{v(x')}\, dx' \tag{IV.4}$$

v is the electron velocity, and x is the distance needed to travel in order to be collected. An example of this calculation for a given electric field can be seen in Fig. IV.7. The transit time gives the temporal representation of when charge has been collected. Likewise, a plot of the derivative of T(x) is shown in Fig. IV.8. This shows that the slope below 0.10

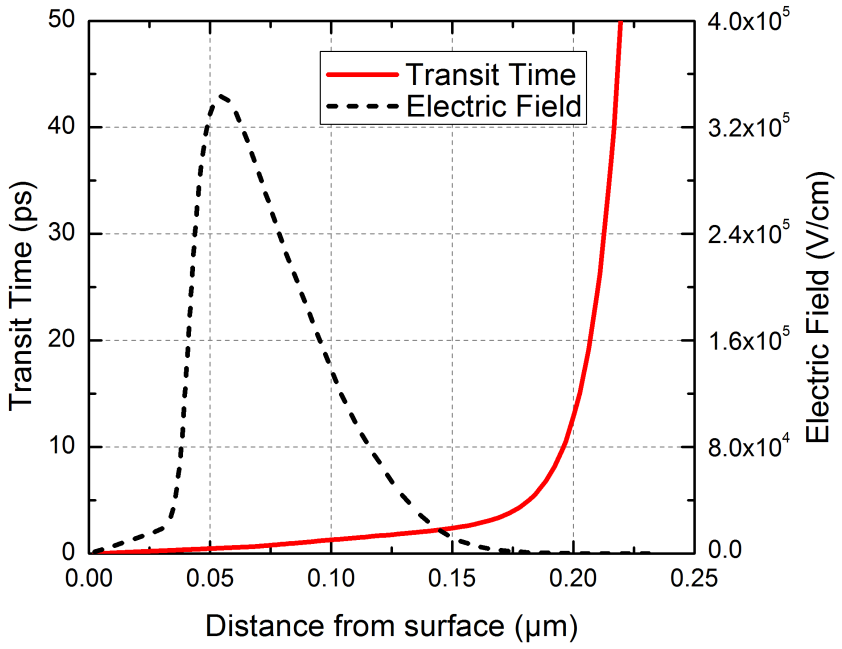

Figure IV.7: Electric field and transit time shown as a function of distance in the 45nm transistor shown previously.

μm is not linear, but has a shape that will be represented in the characteristics of the final calculated current pulse.

Solving for velocity in Eq. IV.4 yields,

$$\frac{dT(x)}{dx} = \frac{1}{v(x)}, \tag{IV.5}$$

which is the change in transit time with respect to distance. Multiplying the charge deposition as a function of distance, i.e., LET_{si}, by the distance over which charge is collected, gives the amount of charge collected. Dividing this value by the time over which the charge is collected results in the current of the system.

$$I = LET_{si} \cdot \frac{dx}{dT} \cdot [1 \cdot 10^{-10}] \tag{IV.6}$$

$1 \cdot 10^{-10}$ represents the change in units between MeV-cm^2/mg and C/cm for Silicon.

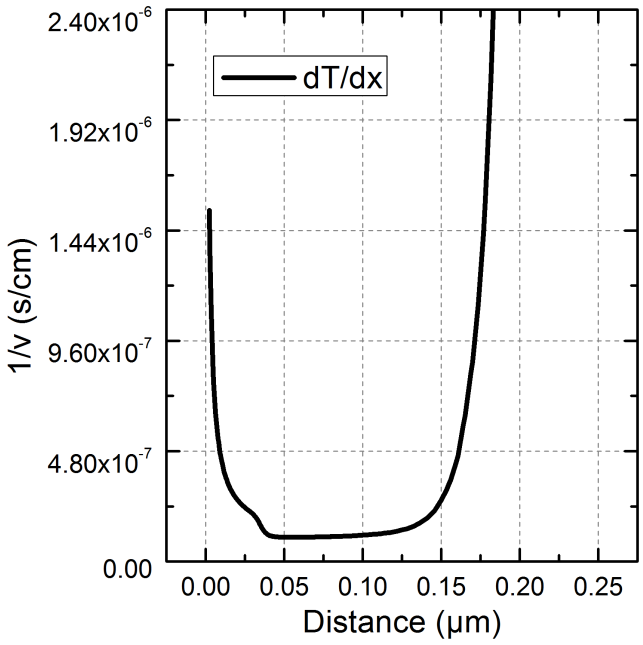

Figure IV.8: dT/dx as a function of position. Data is from the same device as A.1

Substituting Eq. IV.5 into Eq. IV.6 gives a solution that can be plotted vs. time to generate a current pulse using the method described here.

$$I(t) = LET_{si} \cdot v(x(t)) \cdot [1 \cdot 10^{-10}] \tag{IV.7}$$

IV.2.1 Field Perturbation

The previous derivation is valid for simulations where the electric field is not greatly perturbed. Most single-event strikes perturb the depletion region electric field to some extent. The perturbation of the electric field is dependent on many factors including the generation time of the carriers. A result of strikes that perturb the electric field, but do not completely collapse it, is a spreading of the FWHM of the pulse. It occurs because of a decrease in the velocity of carriers in the depletion region, which results in an increase in transit time. This is mainly a function of the perturbed electric field, but also of a change in mobility due to carrier-carrier scattering of the generated charge. A straightforward solution was implemented to resolve the calculated temporal characteristics under conditions where the field

is significantly modulated by the generated charge. This is accomplished by calculating the perturbed carrier velocity and comparing it to the steady-state carrier velocity. TCAD was used to solve the post-strike conditions for this thesis, but for efficiency, a lightweight simulation package can be used in its place. The ratio of the original carrier velocity to the perturbed velocity is represented by FP.

$$FP = \frac{v_{steady-state}}{v_{post-strike}} \tag{IV.8}$$

Using the peak values of the pre and post strike velocities results in a single value for FP, and is the most straightforward to implement. This accounts for the modified electric field and mobility, as well as the generation rate of the model. This is not a fitting parameter, but rather a calculated value of the perturbation of the electric field, and thus the electron velocity due to carrier injection. The formulation appears as,

$$T(x)_{new} = FP \cdot T(x)_{original}, \tag{IV.9}$$

which can essentially be thought of as extending the pulse width to FP times the FWHM of the steady-state calculated pulse. $T(x)_{new}$ replaces the original calculation for $T(x)$, and can be used directly in the formulation of $I(t)$. In Fig. IV.9 an example with FP = 3 is shown. This method creates a very accurate result because it uses the shape of the original pulse, but widens the pulse by the amount of velocity degradation due to carrier generation. This method is more accurate than only using the post strike velocity to generate the pulse shape because the electric field, and thus the velocity, relaxes to a near steady-state condition while the fast transient current pulse is being generated. This creates a pulse that is almost identical in shape to a pulse generated from an unperturbed electric field, but is spread in time to account for degradation in magnitude of the post-strike electric field. An example of pulse spreading is show in IV.10. At each value of LET_{Si} there is a particular value for

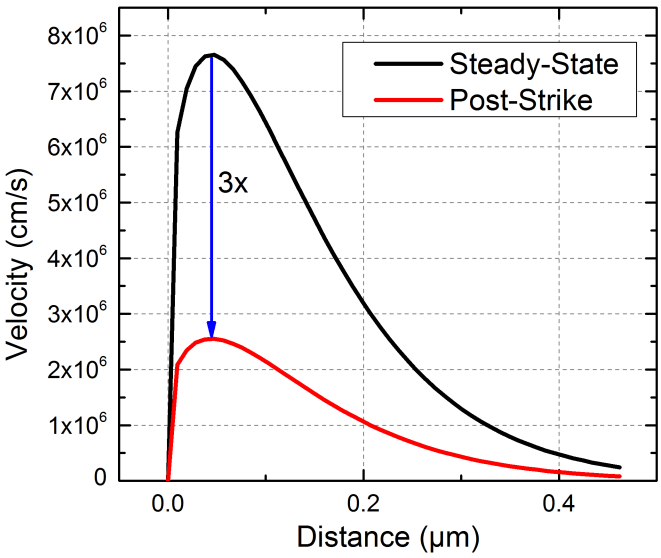

Figure IV.9: Example of the constant FP on a steady-state and post-strike electric field.

FP.

The values of velocity used for the calculation of FP were taken at a radial distance that corresponds to half the maximum of the generation Gaussian. This is 0.5 of the peak density, and is shown as a function of radial distance in Fig. IV.11. For numerical reference for the normalized charge values given in Fig. IV.11, an LET of 1, 5, 10 MeV-cm^2/mg, corresponds to a peak carrier density of $7.8{\cdot}10^{18}$, $3.9{\cdot}10^{19}$, $7.8{\cdot}10^{19}$ cm^{-3} respectively. To show the possible changes in FP as a function of the location where data are extracted, FP as a function of normalized heavy-ion charge density is plotted in Fig. IV.12. Choosing a location that corresponds to 0.5 the peak density, or locations close to this, yield very similar values of FP. At the carrier injection densities of interest ($>1{\cdot}10^{18}$ cm^{-3}), mobility varies only slightly with increased injection, so the main contributor to the change in FP is the electric field, which is given by the derivative of the energy bands in the crystal. The goal when selecting a location for FP is to choose a location in the generation Gaussian that gives an approximate response of the junction as a whole; for the presented technologies, this corresponds to a value of half the generation Gaussian peak. This method is interested in the approximate response of the junction, so values were extracted halfway between both

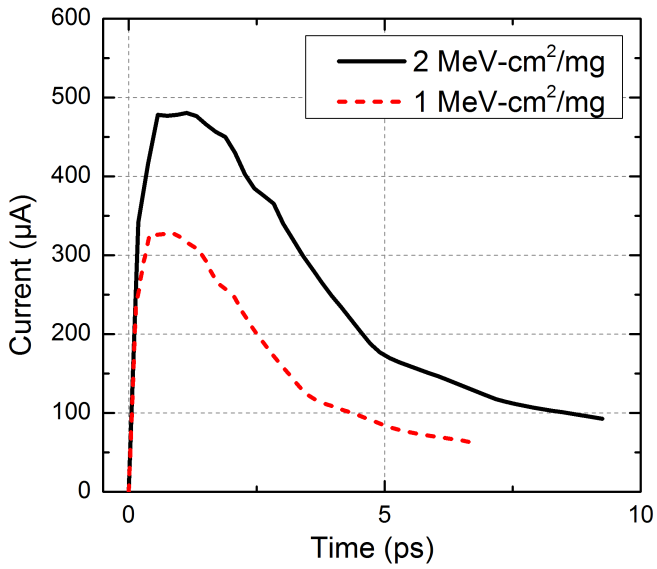

Figure IV.10: Example of pulse spreading for increased energy deposition. The spread in time is due to the decrease in electron velocity due to the perturbed electric field, while the change in magnitude is due to an increase in deposited charge in the collection volume.

extremes. This value may not always be the best answer, but gives a good approximation well inside both extremes.

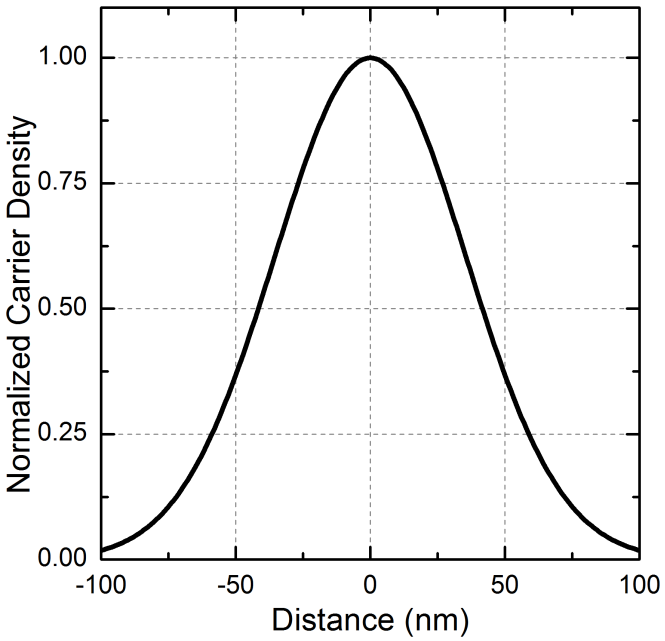

Figure IV.11: Normalized carrier concentration as a function of radial distance. The center of the generation track is at 0 nm.

IV.2.2 Charge Collection Volumes

In order to calculate an accurate magnitude of the current pulse, a method to calculate the LET_{si} is needed. In the most basic treatment, the LET could be taken from a lookup table depending on the environment spectra. However, for a more statistically valid and more accurate sample space, an energy deposition tool is the most appropriate choice. For this work, MRED was used for the calculation of LET_{si} for a given particle. This is accomplished by generating volumes that describe the region that collects charge inside of the FWHM of the fast transient pulse. For modern technologies where "field funneling" is not a major concern, the FWHM of Eq. A.8 does not depend on the exact numerical value of LET_{si}, but depends only on $v(x)$. For the calculations of the geometrical boundaries of the volume set, LET_{si} can be set to 1, as it is only a scaling factor and does not affect the time evolution of the pulse. It appears as,

$$I(t)_{LET=1} = 1 \cdot v(x(t)) \tag{IV.10}$$

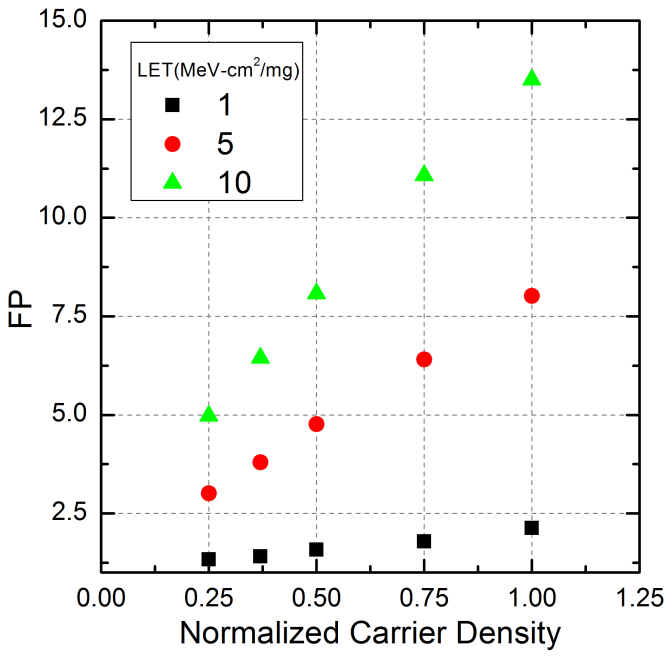

Figure IV.12: FP as a function of the location chosen for the selection off the post strike velocity. A value of 1.0 represents the peak carrier generation due to the heavy-ion.

For older technologies where "field funneling" is a significant factor in charge collection, the FWHM has to be calculated for each value of LET_{si}, because the distance over which the FWHM occurs increases with increased LET_{si}. This increased in distance is what gives rise to "field funneling," but is not a major concern in modern devices because of relatively high doping levels.

Taking the time period that represents the FWHM, and solving for the distance that corresponds to that transit time (Fig. A.1) gives the locations of the top and bottom of the volumes. The location of the top and bottom of the volume is given by,

$$x_{TOP} = x(t_{START}) \tag{IV.11}$$

$$x_{BOTTOM} = x(t_{END}) \tag{IV.12}$$

t_{START} and t_{END} are the beginning and end times of the FWHM of the calculated current

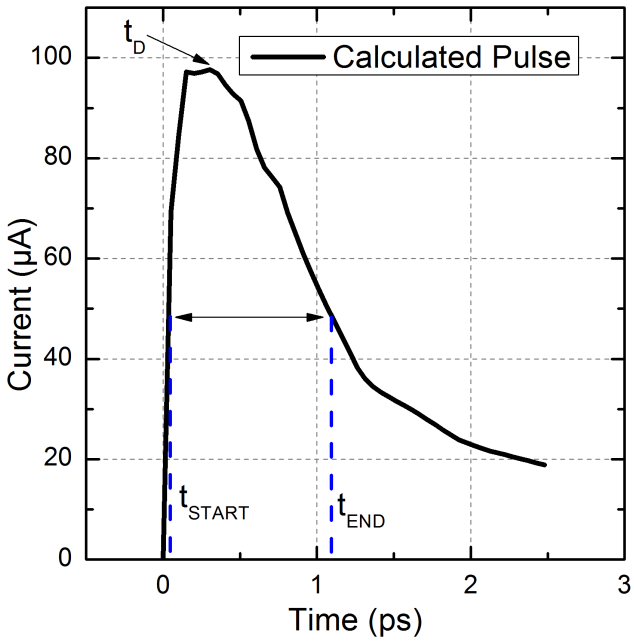

Figure IV.13: Volume Calculation using the FWHM of the calculated fast transient pulse

pulse shown in Fig. IV.13. Using the calculated volume size and location, a value for LET_{Si} can be determined. The most accurate and efficient way to make this calculation is to normalize the FWHM of the current pulse to the total charge deposited in the entire set of volumes for the node of interest. The magnitude of the calculated current pulse is given by setting the integral of the FWHM of $I(t)$ equal to the total charge deposited in the volume set,

$$\int_{t_{START}}^{t_{END}} I(t) = Q_{volumes}. \tag{IV.13}$$

$Q_{volumes}$ is the total charge deposited in the volume set. These volumes can be thought of as 100% efficiency collection volumes. It would not be accurate to attempt to divide up these regions and make the calculations mutually exclusive, because charge can travel from one volume to another, even though the dominant direction of current flow is towards the contact. Substituting Eq. A.6 into Eq. IV.13 yields,

$$\int_{t_{START}}^{t_{END}} LET_{Si} \cdot v(x(t)) \cdot [1 \cdot 10^{-10}] = Q_{volumes} \tag{IV.14}$$

In order to use this directly in the preceding derivations of $I(t)$, Eq. IV.14 is solved for LET_{Si} giving,

$$LET_{Si} = \frac{Q_{volumes} \cdot [1 \cdot 10^{-10}]}{\int_{t_{START}}^{t_{END}} v(x(t))} \tag{IV.15}$$

The width of the volume is given by the device geometry, and should be no larger than the length of the collecting diffusion. More than one volume can be used to describe a region of curvature, and such a set of volumes is shown in Fig. IV.14. For the case of the nMOSFET, the volume set for the drain begins at the field oxide and ends in the center of the channel. Likewise, a volume set for the source could be created by starting at the center of the channel, and ending at the field oxide next to the source.

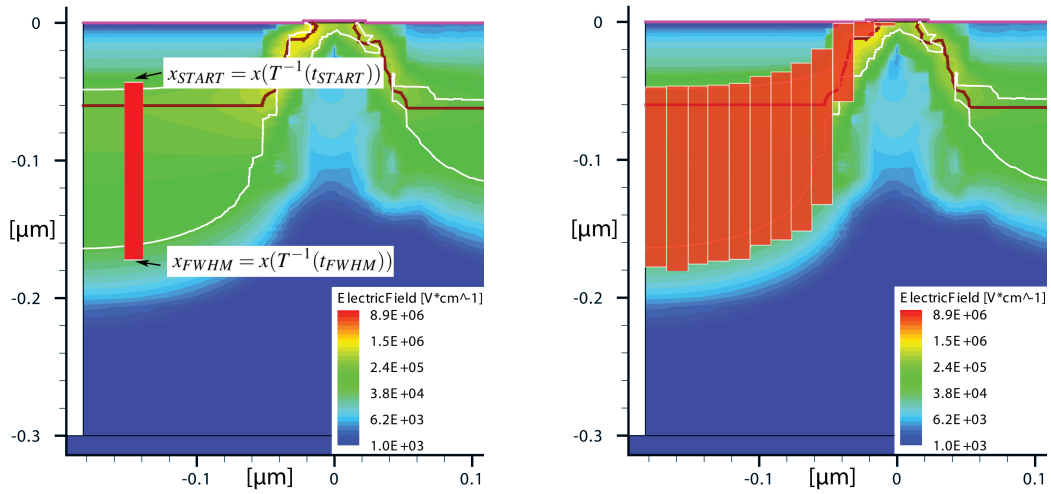

(a) Single volume with the start and end location shown for the FWHM.

(b) Full set of volumes.

Figure IV.14: Single volume and full set of volumes shown on top of a 45-nm transistor biased at 1V.

IV.2.3 Angled Strikes

Angles of incidence should be accounted for in single-event simulations. When an ion of relatively high LET passes through a junction at an off-normal angle, differences in the pulse shape can be observed. For the energy ranges considered here, angle of incidence alters the amount of charge deposited, but not the characteristics of the pulse. This can be

accounted for by using an effective LET and is accurate in the calculations of this method [21]. Fig. IV.15 shows strikes traveling through the drain of a 45-nm nMOSFET biased at 1 V. The “0 Degrees” strike is normal to the contact, while the “45 Degrees” strike makes a 45 degree angle with the surface contact.

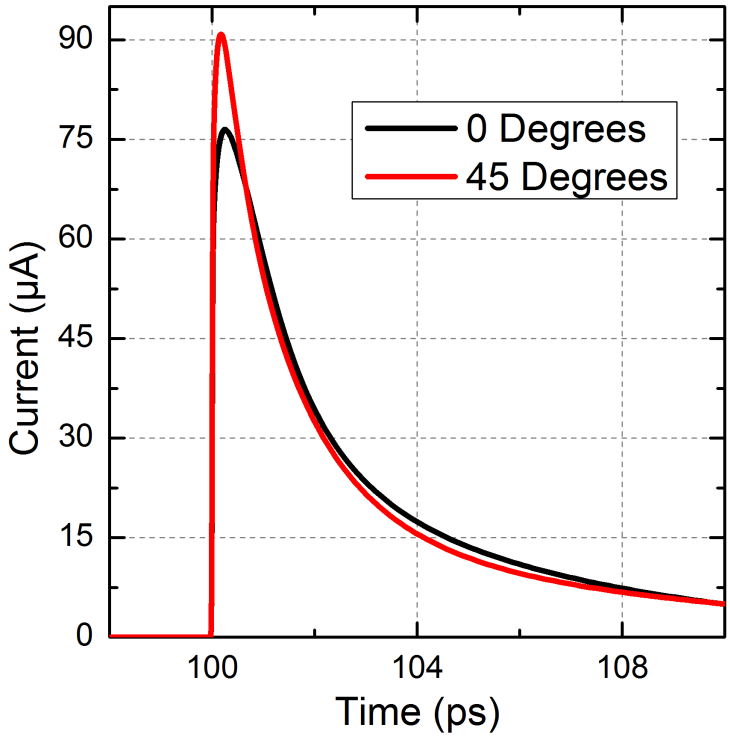

Figure IV.15: Current pulses generated in TCAD for strikes normal to the surface, and at a 45 degree angle with the surface of the drain of a 45-nm transistor.

The FWHM of the two pulses are close in value, even though the amount of deposited charge is not. The major difference between the two pulses is the peak current. Between the two different angles of incidence, there is approximately a 21% difference in peak current. The difference in deposited charge is handled by the charge deposition software, in this case MRED. When particles with the same LET pass through the volume at different angles, they can deposit different amounts of charge. The charge is used to calculate the magnitude of the output pulse, thus handling angles inherently. This can be thought of as an effective LET, where the charge deposted by an angled strike can be equated to

an LET of a normal incidence strike [21]. This allows angled strikes to be calculated in the same way that normal incidence strikes are calculated. So the actual temporal pulse shape characterization remains the same when compared to a strikes that deposits the same amount of charge at normal incidence.

IV.2.4 Range of Validity

Knowing when a model breaks down is crucial to understanding how the model can be used. There is one major attribute required for this method of pulse characterization to be valid. The electric field in the depletion region should not collapse due to the generation of carriers. This has different values depending on the amount of generated charge and the doping of the junction. For many modern technologies, this corresponds to an LET greater than 10 MeV-cm^2/mg.

Technologies with relatively low peak doping profiles ($< 1 \cdot 10^{16}$ cm^{-3}) have a valid LET range that is less, as shown in a simple example. The example uses an epitaxial diode with a lightly doped epitaxial region ($1 \cdot 10^{15}$ cm^{-3}). It consists of a highly doped n+ region, over a low doped epitaxial region, on top of a highly doped substrate. An image of the doping profile in shown in figure IV.16. The method described here gives accurate

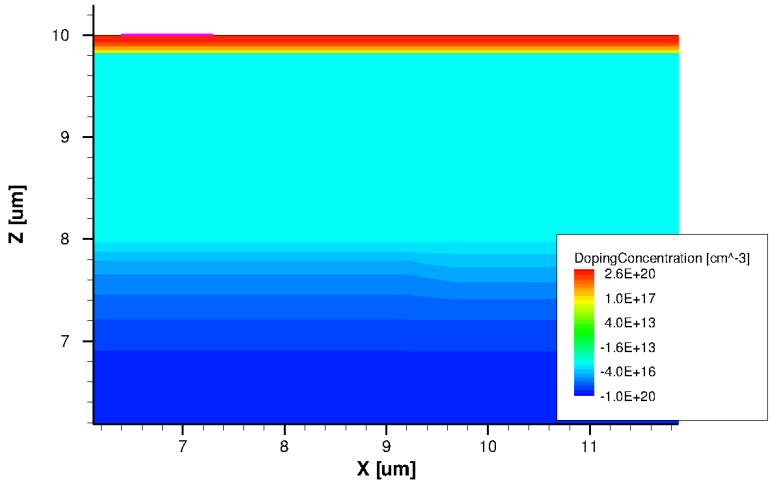

Figure IV.16: Doping profile for an epitaxial diode.

results up to an LET of 2 MeV-cm^2/mg, as shown in Fig. IV.17. Above 2 MeV-cm^2/mg , the electric field present in the epitaxial layer is overwhelmed by the generation of carriers and it collapses. This is a function of the low doping present in the epitaxial region, combined with the heavily doped region below. Diffusion becomes dominant at fairly low injection levels in this region. The diode is reverse biased at 10 V and the thickness of the depletion region is approximately 0.8 μm. This can be seen clearly in Fig. IV.17b as a widening of the simulated pulse well beyond the calculated pulse. A comparison of the calculation compared with TCAD results for an LET of 1 and 10 MeV-cm^2/mg are shown in IV.17. A strong deviation from the calculation can be seen in the higher energy strike, due to the low doped epitaxial region.

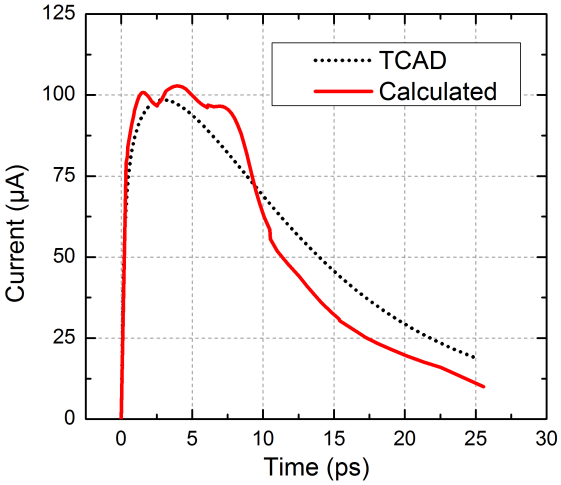

(a) LET 0f 2 MeV-cm^2/mg.

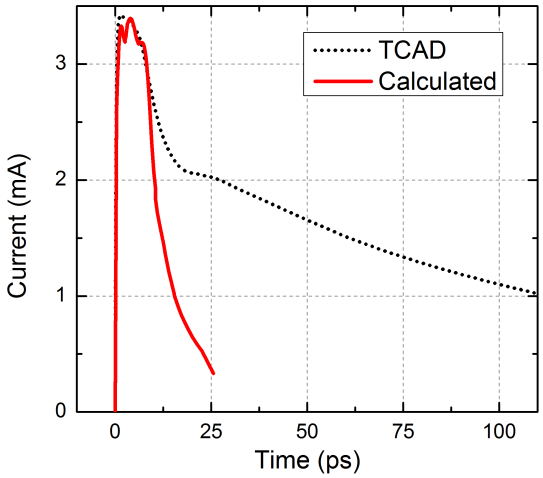

(b) LET of 10 MeV-cm^2/mg.

Figure IV.17: Example of epitaxial diode where the calculation is not valid.

IV.2.5 Method Summary

Four central equations are used in the calculation of this method. The time it takes a carrier at distance x to be collected is obtained from:

$$T(x) = \int_0^x \frac{1}{v(x')}\, dx' \tag{IV.16}$$

The ideal current pulse, assuming no perturbation of the electric field and not knowing an exact value for LET_{Si}, is calculated using:

$$I(t) = LET_{si} \cdot v(x(t)) \cdot [1 \cdot 10^{-10}] \tag{IV.17}$$

The perturbed electric field is accounted for by calculating FP, which alters the steady-state transit time:

$$T(x)_{new} = FP \cdot T(x)_{original} \tag{IV.18}$$

LET_{Si} is calculated using the charge deposited in a set of collection volumes,

$$LET_{Si} = \frac{Q_{volumes} \cdot [1 \cdot 10^{-10}]}{\int_{t_{START}}^{t_{FWHM}} v(x(t))} \tag{IV.19}$$

IV.3 Functional Fitting of Current Pulse Characteristics

The simulation method generates a waveform that is not as smooth as that expected from physical processes (Fg. IV.13). This is because the solution is a simplified 1D calculation of a complex 3D device. Carrier transport is dictated by differential equations that, by nature, equalize any sharp edges appearing in the current pulse.

Because many simulation packages need smooth curves and closed-form solutions to run effectively, these curves can be fit to other functions. A basic fit that has been used frequently is the double exponential[22]. While this function is not perfect for all heavy-ion data, it serves as an example of the accuracy of this method when fitting to functions for higher level circuit simulation. To fit the double exponential, the FWHM and peak values

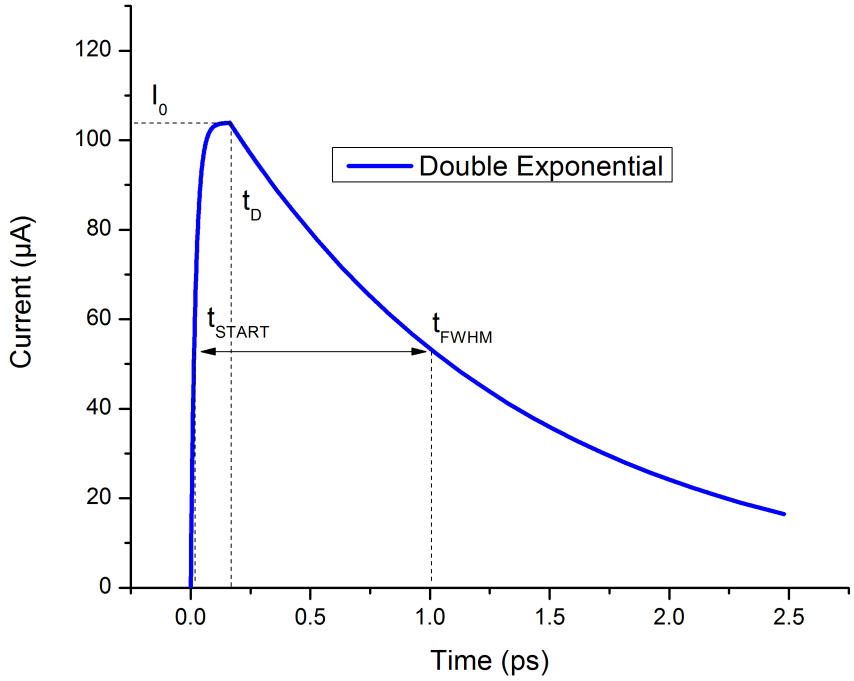

Figure IV.18: Sample double exponential function showing the components that are used to fit the function.

are extracted using the data output from the calculations presented. This is done using the following:

$$I(t) = \begin{cases} I_0 \cdot (1 - e^{-t/\tau}) & \text{for } t < t_D \\ I_0 \cdot (1 - e^{-t_D/\tau})(e^{-(t-t_D/\tau_F)}) & \text{for } t > t_D \end{cases} \tag{IV.20}$$

where I_0 is the peak current, τ_F is the falling time constant, τ_R is the rising time constant, and t_D is the time that the peak value occurs. For device responses that can be well described by fitting the FWHM, Eq. IV.20 is set equal to half the maximum current, which yields values for τ_F and τ_F.

$$\tau_F = \frac{t_{FWHM} - t_D}{ln[2 - 2e^{(t_D/\tau_R)}]} \tag{IV.21}$$

$$\tau_R = \frac{t_{START}}{ln(2)} \tag{IV.22}$$

where t_{START} is the starting time of the FWHM and t_{FWHM} is the end time.

$$I_0 = \frac{\int_{t_{START}}^{t_D} (1 - e^{-t/\tau}) + \int_{t_D}^{t_{FWHM}} (1 - e^{-t_D/\tau})(e^{-(t-t_D/\tau_F)})}{Q_{volumes}} \tag{IV.23}$$

$Q_{volumes}$ is the charge deposited inside the volume set described previously. The solution is closed-form, and can be solved in real time using the charge deposited in the collection volume set.

CHAPTER V

Method Output Comparison and Validation

V.1 Pulse Shapes

The two technologies that were used as demonstration devices were explained in detail in Chapter III. To verify the accuracy of the simulation method, a variety of LET values and incident angles were run on both devices. As can be seen in the results, these two devices have different fast transient responses, and give a range of examples from which to validate this process.

The first set of data is a series of strikes on the 45-nm nMOSFET transistor. These strikes were normal to the drain and the drain was biased at 1 V. The source and substrate were grounded. The strikes were centered inside the drain, and traveled well into the substrate. The track radius was 50 nm and the characteristic value of the generation Gaussian was approximately $2 \cdot 10^{-13}$ s. The LET of the generation track was stepped from 1 to 10 MeV-cm^2/mg covering the entirety of the defined solution space. This is not a hard limit, and strikes with a higher LET will start to vary, eventually diverging from the calculated pulse shape. Fig. V.1 shows the series of strikes in the 45-nm transistor.

While TCAD and the presented method due not generate identical results, the general shape of the fast transient pulse is closely matched. As discussed previously, all of the presented pulses can be fit to closed-form equations for implementation into higher level simulations. This would also eliminate some of the jagged nature of extracting data from a finite element model. At an LET greater than 10 MeV-cm^2/mg, the electric field is so greatly perturbed by the generation of carriers that the response is no longer accurately predicted by this method. This value is accurate for the devices presented, but different doping profiles could have limits that are slightly higher or lower. The only way to confidently set

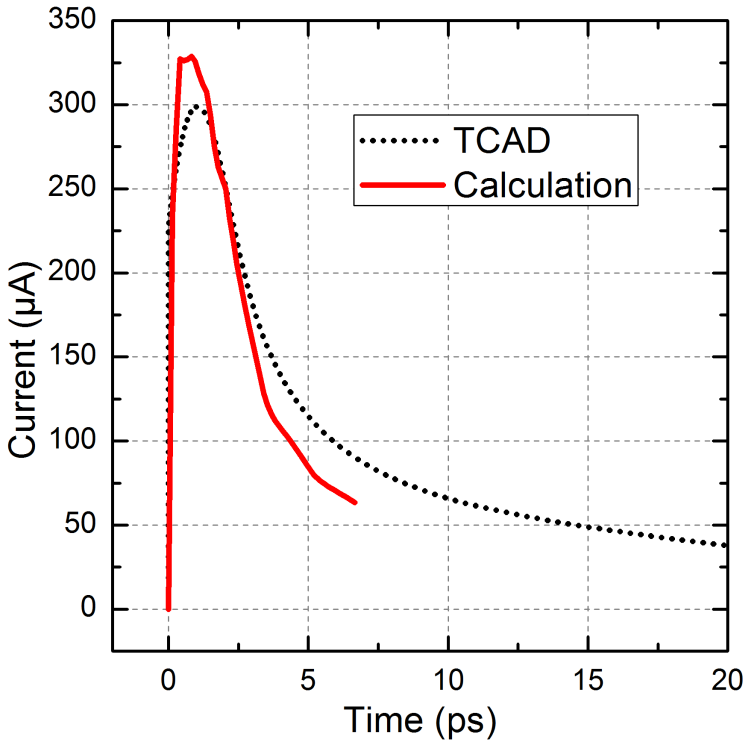

(a) LET of 1 MeV-cm^2/mg.

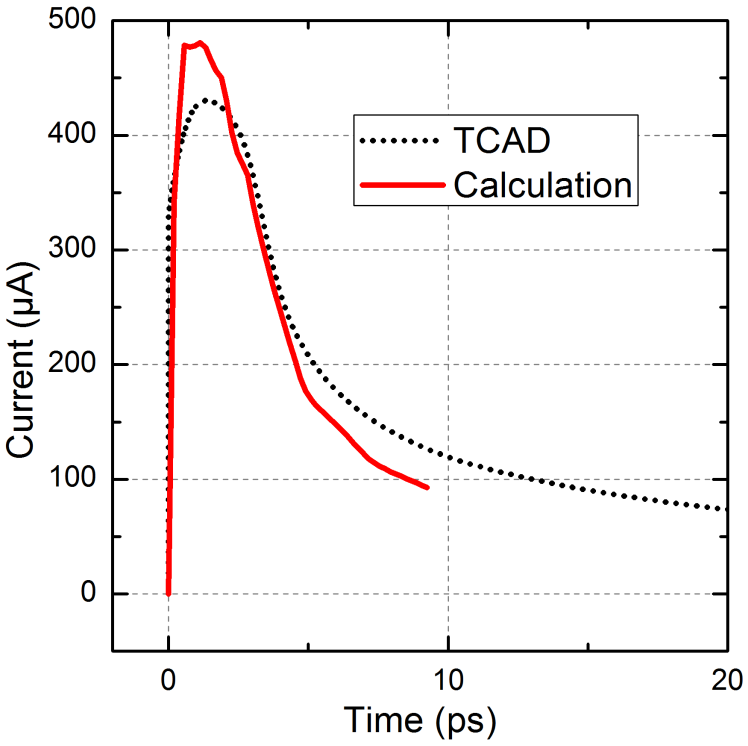

(b) LET of 2 MeV-cm^2/mg.

Figure V.1: Calculation comparison for an LET of 1 and 2 MeV-cm^2/mg on a 45nm transistor.

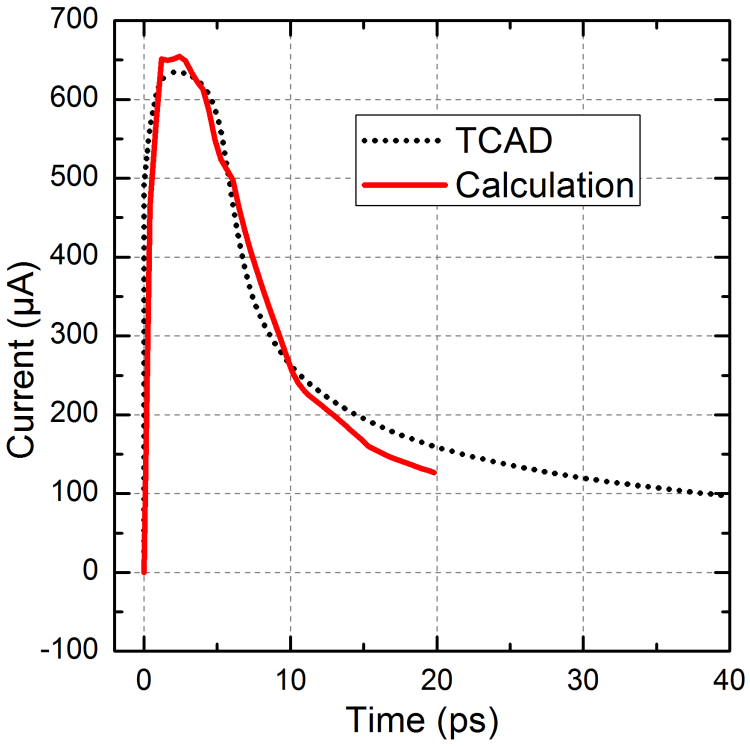

(a) LET of 5 MeV-cm^2/mg.

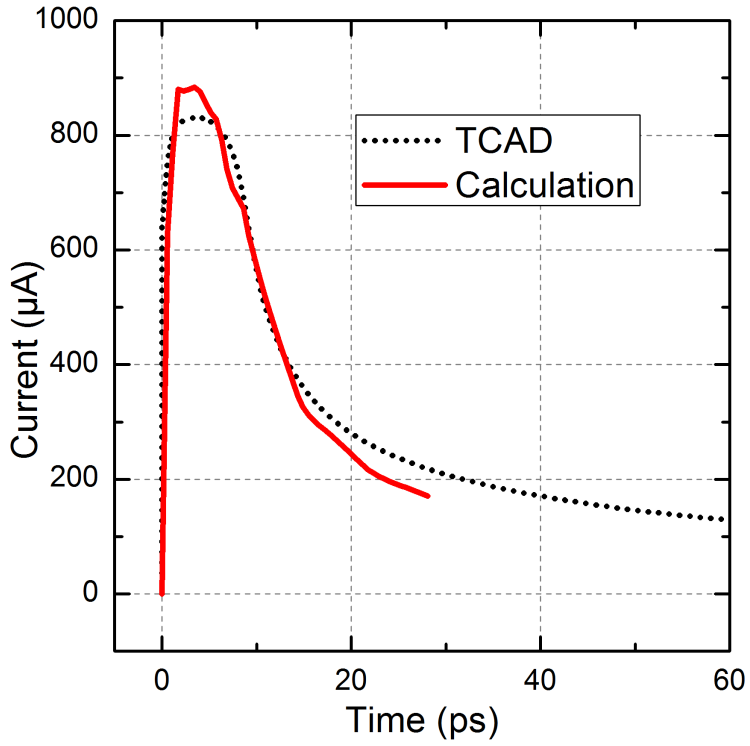

(b) LET of 10 MeV-cm^2/mg.

Figure V.2: Calculation comparison for an LET of 5 and 10 MeV-cm^2/mg on a 45nm transistor.

this interval is to understand the electric fields present in the biased device, thus knowing when it is severely perturbed. To reiterate, this issue occurs when the reverse biased depletion region collapses during the injection of carrier from an ion strike. As long as the depletion region electric field is sufficiently strong to cause a significant drift current, this model will be valid.

Similar results for the large area diode discussed earlier, Chapter III, are shown in Fig. V.3. The LET was varied in the same manner as in the 45-nm nMOSFET, using an identical track structure and characteristic generation Gaussian. The track was normal to the surface, and the strike took place in the center of the device. The junction was reverse biased at 10 V. The results show that this method once again matches very well to the full 3D TCAD solution, while significantly reducing solution time, which is detailed in Section V.3.

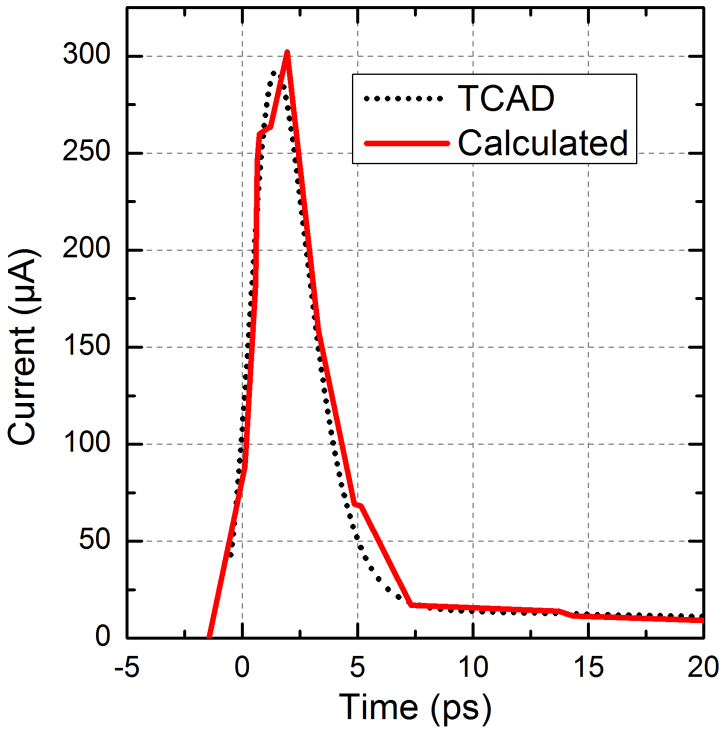

(a) LET 0f 1 MeV-cm^2/mg.

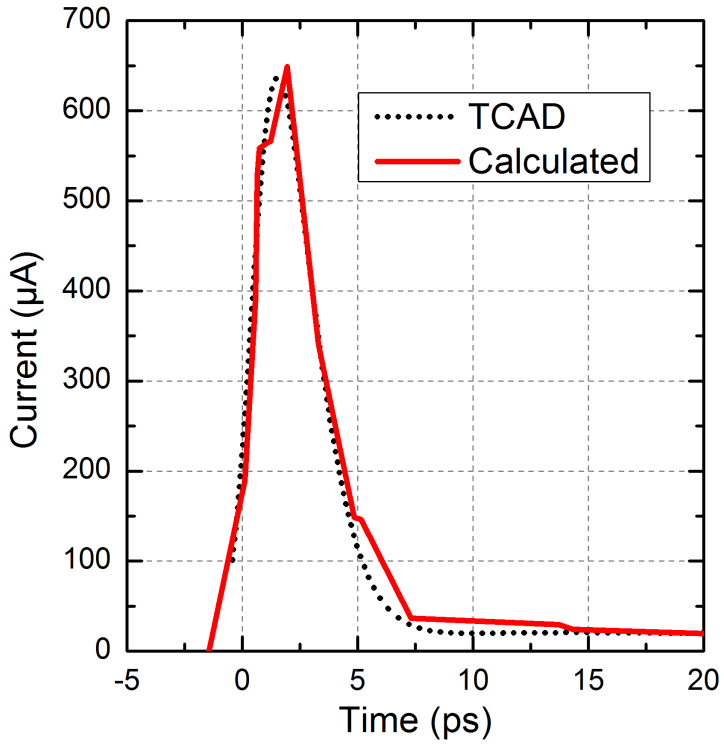

(b) LET of 2 MeV-cm^2/mg.

Figure V.3: Calculation comparison for an LET of 1 and 2 MeV-cm^2/mg on a large area diode.

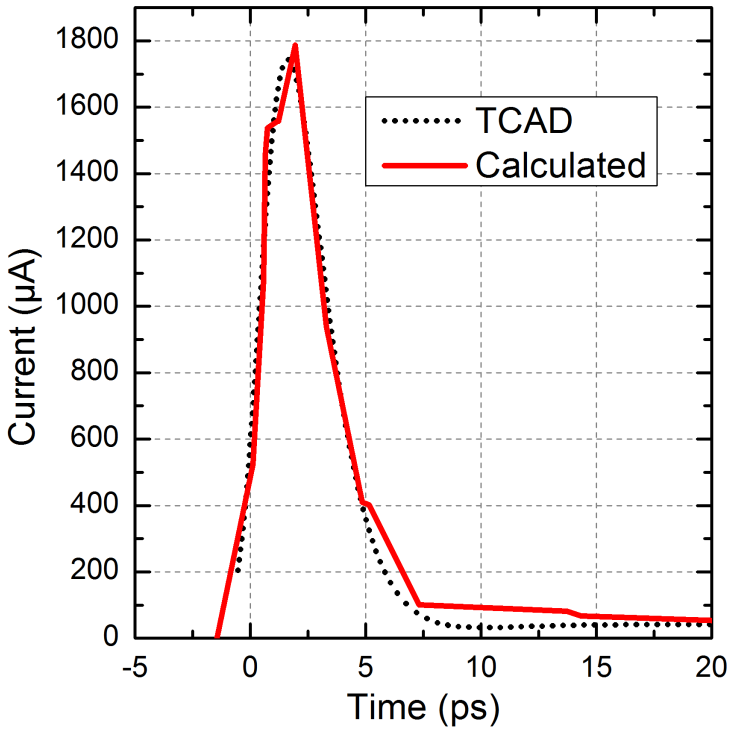

(a) LET of 5 MeV-cm^2/mg.

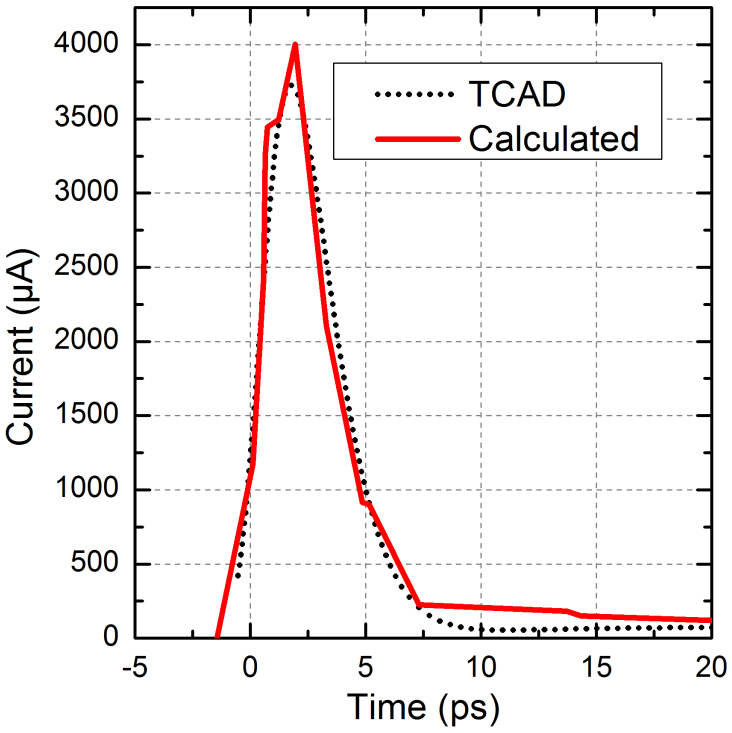

(b) LET of 10 MeV-cm^2/mg.

Figure V.4: Calculation comparison for an LET of 5 and 10 MeV-cm^2/mg on a large area diode.

V.2 Circuit Simulations

Pulse shapes were shown in the previous section to closely match the full TCAD solution. In many circuits, the slight differences in pulse shape do not result in a significant changes in the accuracy of circuit-level simulations. To show this assertion, a basic storage element was simulated in Cadence Virtuoso Spectre Circuit Simulator[23]. It consisted of a transmission gate on the input, a storage and feedback loop, as well as an output inverter. The circuit can be seen in Fig. V.5. Current was injected using the bias dependent compact model published by Kauppila et al.[2], which helps eliminate the possibility of injecting unphysical amounts current into the circuit. This model is a modified current source that responds dynamically to circuit conditions. The current source checks the bias condition on the connected node, and adjusts the amount of injected current accordingly. If an ideal current source was implemented instead of the bias dependent model, it would be possible to inject more current than a real circuit could produce, causing the results to be skewed.

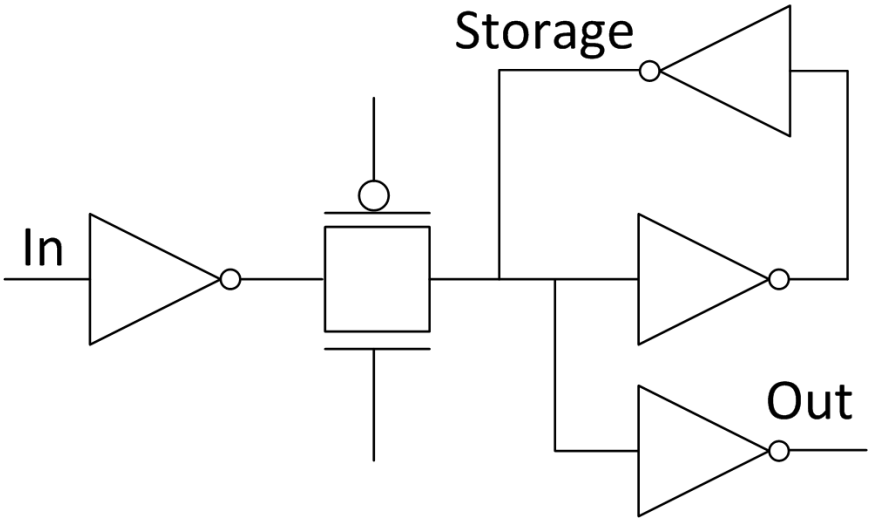

Figure V.5: Latch circuit used to show the accuracy of the calculated pulses.

To inject the correct current pulse waveform, the bias dependent model has to be calibrated to the device under test. For comparison, pulses were calibrated using TCAD results and using the method presented. The threshold for upset was calculated by increasing

the charge inside the generated pulse until the storage node flipped. The two values of critical charge were then compared to determine the amount of error introduced by this method. Table V.1 shows that there was a 1.61% difference in the two solutions, while providing significant efficency gains when compared directly to the 3D TCAD solution, and improvements in solution time of 5 to 100 times can be seen when compared to 1D TCAD, see Section V.3.

Method	Q_{crit} (pC)	Difference (pC)	Difference (%)
TCAD	$5.709 \cdot 10^{-3}$	-	-
Presented Method	$5.617 \cdot 10^{-3}$	$9.2 \cdot 10^{-5}$	1.61

Table V.1: Circuit simulation results for method verification.

There are circuits for which the pulse shape calibration presented in this work has little effect, and in such circuits this method does not have significant utility. Circuits that depend mainly on the total collected charge are an example of this case, such as a DRAM cell. While these situations should be considered, using the calculations shown here does not negatively alter the results in any case, but could improve accuracy significantly over not calibrating the pulse shape appropriately.

V.3 Computation Time Comparison

The time to compute a solution has been compared throughout this work, and this section substantiates the claims with details of the device simulations being performed. Three types of simulations were performed, 3D TCAD, 1D TCAD, and the presented method. The reported time excludes bias condition simulations that have to be run in all of the compared methods. They are needed for the presented method in order to extract values of electric field. The bias simulation time for 1D, 2D, and 3D models, using the hardware described, are approximately 30 s, 4 min, and 14 min respectively.

Two 3D TCAD devices were simulated in this work; the presented nMOSFET and

large area diode described previously. The nMOSFET has 37,437 mesh points requiring solution, and was simulated on an 8 core Intel Nehalem processor. This simulation took 6.25 hours, and required 3.4 GB of memory. The large area diode has 220,000 mesh points, due mainly to its large dimensions, and was simulated on an 8 core Intel Nehalem processor. This simulation took 11.7 hours, and required 5.2 GB of memory.

Two 1D TCAD devices were simulated to match a 1D slice through the presented nMOSFET and large area diode. The nMOSFET has 513 mesh points requiring solution, and was simulated on an single core Intel Nehalem processor. This simulation took 4.5 minutes, and required 800 MB of memory. The large area diode had an identical mesh structure, and solution times in 1D.

In comparison, the presented method was run on a single core Intel Nehalem processor, consumed less than 100 MB of memory, and took 6 seconds to complete. This does not include the MRED simulation time, which can range from hundreds of events per second, to minutes per event for rare events. To implement the method as described here, one MRED event is required per calculated current pulse. A large amount of the 6 second run time is the overhead cost of loading software, which only occurs once per session. This allows 100 events to be calculated in 15 seconds. All of these values have been summarized in Tbl. V.2.

Method	Threads	Memory (GB)	Time for One (m)	Time for One Hundred (m)
3D TCAD nMOSFET	8	3.4	373	37,300
3D TCAD diode	8	5.2	702	70,200
1D TCAD (both)	1	1	4.5	450
Presented Method	1	0.1	0.1	0.25

Table V.2: Calculation time for TCAD and the presented method.

CHAPTER VI

Summary

VI.1 Conclusions

The presented method is able to calculate pulse shapes efficiently, enabling their use in fast simulations, which can be crucial for creating tools used by circuit designers. As technologies continue to scale, the ability to capture the response of a circuit element during a design work flow, allows for single event upsets to be accounted for.

The model described here is accurate up to 10 MeV-cm^2/mg, and as discussed previously, this is not a hard limit, but an estimated value for modern technologies. This limit means that the results from these calculations can apply not only to terrestrial environments, but to space applications as well. Using the presented method for strikes that deposit charge outside the demonstrated range of validity will become more inaccurate as the amount of charge is increased. However, calibrating a model with this method, even outside of the given limits, still provides a more accurate solution than assuming a pulse shape without proper calibration.

The output from this work is quite accurate when compared to the full finite element solution from the heavy-ion command in TCAD. Even the small differences in outputs can be further be eliminated by assuming a function that closely resembles the output response of the device. For most circuits, the slight differences in these pulse shapes do not significantly alter the statistics of the circuit's single event hardness. However, the decreased time to obtain a solution allows designers to utilize a calibrated device response for simulations. An example of computation time for both TCAD and the presented model can be seen in Table V.2.

This model is ideal, not accounting for higher level circuit effects that could alter pulse shapes. This method is meant to be a calibration for models that take into account these

other effects. An example of a model that can be used in conjunction with the presented method is the biased dependent model[2].

The accuracy and time advantages of this method are described. These aspects are the main utility of this work, and the simulation method is useful as a stand alone component, or as a system of models to simulate the response of a circuit to incident radiation. This allows for more confidence that the pulse has been represented appropriately by simulation. This leads to accurate simulations that can be implemented with significantly less overhead than alternative methods, i.e., TCAD.

VI.2 Future Work

The limitations of this method have been detailed in section IV.2.4. These limitations also give direction going forward with this method of pulse shape calibration. This method needs to be extended to all values of LET, doping levels, and circuit conditions. The most viable candidate for this is a simulation where the current on the struck node is solved in real time with the circuit simulation. This can already be accomplished using mixed-mode simulations in TCAD, but is extremely computationally expensive.

One solution is to find a way to solve a time based simulation in real time with the circuit simulation. Both 3D and 2D finite element solutions are too slow to be used in series with circuit level simulations, but 1D simulations may just be fast enough to implement. So the goal would be to find a way to solve an ion strike using one or a collection of 1D solutions to quantify the shape of the resultant current pulse. A related, but different, approach was shown in [24]. If the strike is well collimated due to the ambipolar forces keeping opposite charges together, a solution along the ion track could be a viable solution to represent the major characteristics of the pulse. Assuming a cylindrical carrier distribution of equal density, a chord taken directly down the center of the column would be fairly indicative of how charge was moving inside of the plasma. Improvements in this model's ability to handle a variety of conditions would be the goal going forward to increase the utility of this

method.

Appendices

Appendix A

Discrete Time Method Derivation

A discrete time derivation of the presented calculations is given to help ease the implementation of the presented simulation method. The following equations can be directly implemented, but are significantly more complex that the continuous time solution.

These terms are used in derivation of the discrete time solution:

Data Slice 1D series of extracted device data taken at the slice location. This is identical to the 1D chord, and for most device geometries, is a vector normal to the contact. It should contain the following values: doping levels, electric field, and mobility values as a function of distance.

Slice Location Location in the device model where the data for the calculation is extracted. This should begin at the collection contact, and terminate well into the device.

Device Model Geometry, doping profiles, and simulated bias conditions for the device of interest. For this thesis TCAD was used, but is not a requirement.

m The discrete index variable for the dataset. $m = 0, 1, 2, \ldots$, dimensionless.

v(m) Velocity of carriers at the location corresponding to value m, in units of cm/s.

x(m) Distance of value m from the collecting diffusion, specifically the edge of the depletion region inside of the collecting diffusion which is analogous to the current plane in section IV.1.1, in units of cm.

T(m) A function that returns the time it takes for a carrier at distance $x(m)$ to reach the current plane, location $x(0)$, i.e., be collected, in units of s.

$\mathbf{T^{-1}}$(t) Inverse function of T(m), returns the value of m that takes time t to reach the current plane, dimensionless. Example values are shown in Tbl. A.1.

m	T(m)	$T^{-1}(T(m))$
0	1 ps	0
1	1.2 ps	1
2	1.3 ps	2
3	1.6 ps	3
4	2 ps	4

Table A.1: Example of T(m) and $T^{-1}(m)$.

Charge(a,b) Amount of charge deposited between to points a and b, in units of C.

LET$_{si}$ Charge per unit distance, in units of MeV-cm^2/mg.

Transit time is defined here as the time it takes a carrier at a given distance to be collected. For the example of an nMOSFET, it is the time it takes an electron to travel from its generation location to the current plane along the data vector. The function that calculates this value is given by integrating the distance traveled divided by the velocity of the carrier.

$$T(m) = \sum_{j=0}^{m} \frac{x(j+1)-x(j)}{v(j)}, \quad j = 0,1,....,m. \tag{A.1}$$

v is the electron velocity, x is the distance needed to travel in order to be collected, j is a temporary counting variable for the summation, and m is the dimensionless index for the data sequence. These discrete mathematics were calculated using formulations in [25]. This summation has to be calculated for every point m in the data sequence. This generates a dataset that has the transit time as a function of distance. An example of this calculation for a given electric field can be seen in Fig. A.1. Using the data set shown in Fig. A.1, choosing an index value $m = 103$ corresponds to a distance $x(103) = 0.10$ μm which is the distance deposited charge has to travel in order to reach the current plane, $x(0)$. The corresponding value of $T(103) = 1.29$ ps, is the amount of time it takes charge deposited at $x(103)$ to reach the current plane. The transit time gives the temporal representation of when charge has been collected. Likewise, a plot of the derivative of T(m) is shown in Fig.

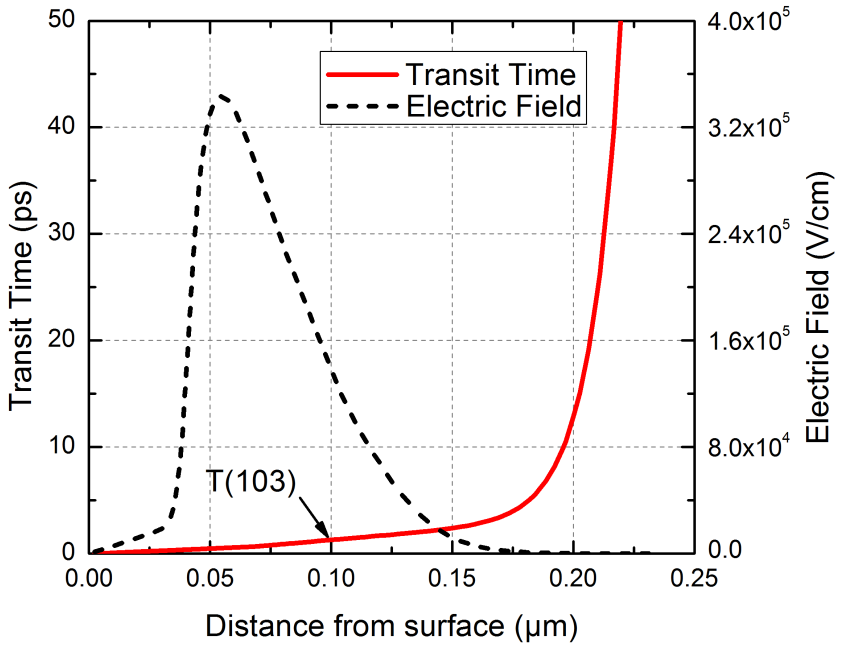

Figure A.1: Electric field and transit time shown as a function of distance in the 45nm transistor shown previously.

A.2. This shows that the slope below 0.10 μ[m is not linear, but has a shape that will be represented in the characteristics of the final calculated current pulse.

A value for the magnitude of the current pulse needs to be determined. The first step is to find the amount of charge that is deposited between two points along the distance vector. Assuming that a value for LET is known, this equation is given by

$$Charge(x(m),x(m+1)) = LET_{si}\cdot[x(m+1)-x(m)]\cdot[1\cdot 10^{-10}] \tag{A.2}$$

$1\cdot 10^{-10}$ represents the change in units between MeV-cm^2/mg and C/cm for Silicon. Dividing the amount of charge by the time over which it is collected results in a value for the rate of charge collection, or current.

$$I(m) = \frac{Charge(x(m),x(m+1))}{T(m+1)-T(m)} \tag{A.3}$$

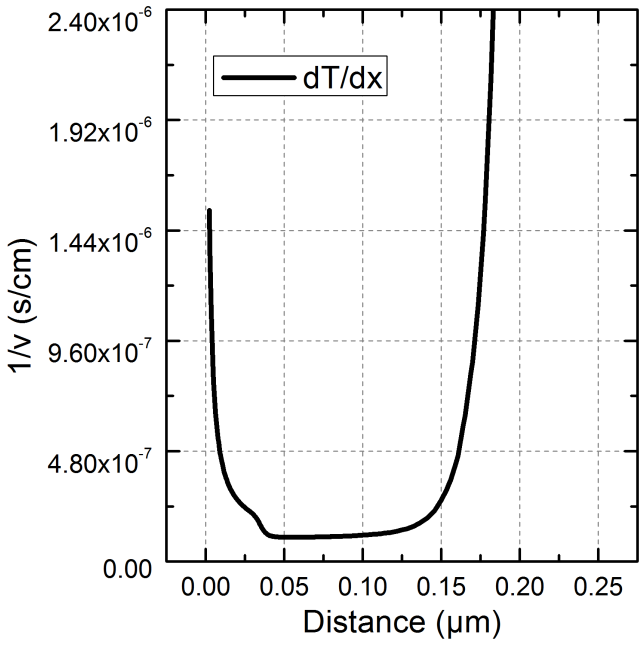

Figure A.2: dT(m)/dx as a function of position. Data is from the same device as A.1

Substituting Eq. A.2 into Eq. A.3 reduces to the LET_{Si}, in MeV-cm^2/mg, times the change in distance, divided by the difference in transit time between successive points (Eq. A.4).

$$= LET_{si} \cdot \frac{\Delta x(m)}{\Delta T(m)} \cdot [1 \cdot 10^{-10}] \tag{A.4}$$

Distance divided by the time is the average velocity of the deposited charge at value m in the data sequence.

$$\frac{\Delta x(m)}{\Delta T(m)} = v(m) \tag{A.5}$$

Substituting Eq. A.5 into Eq. A.4 yields a simple expression for the current as a function of distance (Eq. A.6).

$$I(m) = LET_{si} \cdot v(m) \cdot [1 \cdot 10^{-10}] \tag{A.6}$$

The last transformation is to alter Eq. A.6 such that it can be plotted as a function of time. This is accomplished by using an inverse of the transit time function (Eq. A.1), to

calculate a value in the data set given a time (Eq. A.7).

$$T^{-1}(t) = m \tag{A.7}$$

Eq. A.8 is the final solution that can be plotted vs. transit time to generate a current pulse using the method described here.

$$I(t) = LET_{si} \cdot v(\,T^{-1}(t)\,) \cdot [1 \cdot 10^{-10}] \tag{A.8}$$

REFERENCES

[1] R. Reed, "Fundamental mechanisms for single particle-induced soft errors," *Nuclear and Space Radiation Effects Conference Short Course Notebook*, 2008.

[2] J. Kauppila, A. Sternberg, M. Alles, A. Francis, J. Holmes, O. Amusan, and L. Massengill, "A bias-dependent single-event compact model implemented into bsim4 and a 90 nm cmos process design kit," *IEEE Trans. Nucl. Sci.*, vol. 56, no. 6, pp. 3152 –3157, Dec. 2009.

[3] G. J. Brucker, R. Smeltzer, W. A. Kolasinski, and R. Koga, "Soft error dependence on feature size," *IEEE Trans. Nucl. Sci.*, vol. 31, no. 6, pp. 1562 –1564, Dec. 1984.

[4] B. Sierawski, M. Mendenhall, R. Reed, M. Clemens, R. Weller, R. Schrimpf, E. Blackmore, M. Trinczek, B. Hitti, J. Pellish, R. Baumann, S.-J. Wen, R. Wong, and N. Tam, "Muon-induced single event upsets in deep-submicron technology," *IEEE Trans. Nucl. Sci.*, vol. 57, no. 6, pp. 3273 –3278, Dec. 2010.

[5] Synopsys, "Technology computer aided design (version 2009.06-c)," http://www.synopsys.com/tools/tcad/Pages/default.aspx.

[6] R. Doering, *Handbook of Semiconductor Manufacturing Technology, Second Edition*. CRC Press, 2007.

[7] M. Buehler and B. Blaes, "Alpha-particle sensitive test srams," *IEEE Trans. Nucl. Sci.*, vol. 37, no. 6, pp. 1849 –1854, Dec. 1990.

[8] D. Neamen, *An Introduction to Semiconductor Devices*. McGraw-Hill Science/Engineering/Math, 2005.

[9] H. D. Young and R. A. Freedman, *University Physics with Modern Physics with Mastering Physics (11th Edition)*. Addison Wesley, 2003.

[10] L. Edmonds, "Electric currents through ion tracks in silicon devices," *IEEE Trans. Nucl. Sci.*, vol. 45, no. 6, pp. 3153 –3164, Dec. 1998.

[11] ——, "A theoretical analysis of steady-state charge collection in simple diodes under high-injection conditions," *IEEE Trans. Nucl. Sci.*, vol. 57, no. 2, pp. 818 –830, Apr. 2010.

[12] K. Warren, A. Sternberg, J. Black, R. Weller, R. Reed, M. Mendenhall, R. Schrimpf, and L. Massengill, "Heavy ion testing and single event upset rate prediction considerations for a dice flip-flop," *IEEE Trans. Nucl. Sci.*, vol. 56, no. 6, pp. 3130 –3137, Dec. 2009.

[13] R. Weller, M. Mendenhall, R. Reed, R. Schrimpf, K. Warren, B. Sierawski, and L. Massengill, "Monte carlo simulation of single event effects," *IEEE Trans. Nucl. Sci.*, vol. 57, no. 4, pp. 1726 –1746, Aug. 2010.

[14] I. Synopsys, "Three-dimensional simulations of 45-nm technology cmos devices," Mountain View, C.A., 2008.

[15] C. S. Park, B. J. Cho, L. J. Tang, and D.-L. Kwong, "Substituted aluminum metal gate on high-k dielectric for low work-function and fermi-level pinning free," in *IEDM Tech. Dig.*, Dec. 2004, pp. 299 – 302.

[16] A. Kobayashi, A. Sternberg, L. Massengill, R. Schrimpf, and R. Weller, "Spatial and temporal characteristics of energy deposition by protons and alpha particles in silicon," *IEEE Trans. Nucl. Sci.*, vol. 51, no. 6, pp. 3312 – 3317, Dec. 2004.

[17] X. Zhu, L. Massengill, and C. Cirba, "The effects of nonphysical carrier velocities in high-gradient single event track simulations," *IEEE Trans. Nucl. Sci.*, vol. 47, no. 6, pp. 2568 –2574, Dec. 2000.

[18] L. Artola, G. Hubert, S. Duzellier, and F. Bezerra, "Collected charge analysis for a new transient model by tcad simulation in 90 nm technology," *IEEE Trans. Nucl. Sci.*, vol. 57, no. 4, pp. 1869 –1875, Aug. 2010.

[19] D. Humphreys and A. Moseley, "Gainas photodiodes as transfer standards for picosecond measurements," *Proc. IEE*, vol. 135, no. 2, pp. 146 –152, Apr. 1988.

[20] T. Ezaki, G. Suzuki, K. Konno, O. Matsushima, Y. Mizukane, D. Navarro, M. Miyake, N. Sadachika, H. J. Mattausch, and M. Miura-Mattausch, "Physics-based photodiode model enabling consistent opto-electronic circuit simulation," in *Int. Electron Devices Meeting*, Dec. 2006, pp. 1 –4.

[21] J. Pickel, "Single-event effects rate prediction," *IEEE Trans. Nucl. Sci.*, vol. 43, no. 2, pp. 483 –495, Apr. 1996.

[22] G. C. Messenger, "Collection of charge on junction nodes from ion tracks," *IEEE Trans. Nucl. Sci.*, vol. 29, no. 6, pp. 2024 –2031, Dec. 1982.

[23] Cadence, "Virtuoso spectre circuit simulator (version ic 6.1.3.500)," http://www.cadence.com/products/cic/Pages/default.aspx.

[24] D. Fulkerson and E. Vogt, "Prediction of soi single-event effects using a simple physics-based spice model," *IEEE Trans. Nucl. Sci.*, vol. 52, no. 6, pp. 2168 – 2174, Dec. 2005.

[25] S. S. Epp, *Discrete Mathematics with Applications*. Brooks Cole, 2003.